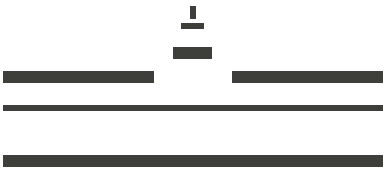

Westfälische
Wilhelms-Universität
Münster

Fach: Mathematik

Comparison of optimization approaches in high-definition transcranial current stimulation in the mammalian brain

Masterarbeit

im Fachbereich Mathematik und Informatik
der Mathematisch-Naturwissenschaftlichen Fakultät
der Westfälischen Wilhelms-Universität Münster

eingereicht von

Simon Homölle

– 2015 –

Dekan:	Prof. Dr. Martin Stein
Erster Gutachter:	PD Dr. Carsten Wolters (Universität Münster)
Zweiter Gutachter:	Prof. Dr. Martin Burger (Universität Münster)

Abstract

Brain stimulation via transcranial direct current stimulation (tDCS) is a non-invasive technique to alternate brain activities through constant current injection. Reaching the right intensity and direction at a specific target in the brain to reach inhibitory or exhibitory currents is the main problem in tDCS-stimulation. In the past different kind of approaches were used to optimize stimulation protocols. In this thesis we will compare four approaches and give an overview over their advantages and disadvantages. To do so we will use two highly realistic FEM head models of a human and a ferret.

Keywords: FEM, volume conduction, optimization, tDCS,

Acknowledgements

I want to thank everyone who made my master studies and this thesis possible, especially:

- My thesis supervisor PD. Dr. rer. nat. Carsten Hermann Wolters for introducing me to the mathematical side of neuroscience and giving me the opportunity to work in his international work group.
- My thesis supervisor Prof. Dr. Martin Burger for giving very profounded lectures about applied mathematics and great input for this thesis.
- Sven Wagner for the great discussions and providing all the relevant knowledge for tDCS.
- Prof. Dr. Christo Pantev for leading and developing a great institute.
- Johannes Vorwerk, Ümit Aydin, Andreas Nüßing, Maria Carla Piastra for nice discussion and scientific input.
- Felix Lucka for providing crucial input for coding some algorithms.
- My collaboration partners from the working group of Prof. Christoph Herrmann and Prof. Andreas Engels. Especially Dr. Florian Pieper for providing the relevant data and knowledge about ferrets.
- My whole family for their unconditional mental and financial support over the past 5 years.
- Finally, I want to thank my long-term girlfriend Kristin for continuous support and understanding even in times where things didn't look promising.

This work was supported by the German Research Foundation (DFG) in the scope of the priority program SPP1665, project WO1425/5-1.

Contents

1 Introduction

1.1 Overview

In the past, a lot of techniques for brain stimulation have been developed, namely transcranial magnetic stimulation (TMS), repetitive transcranial magnetic stimulation, transcranial alternating current stimulation (tACS), and transcranial direct current stimulation(tDCS).
First of all there are a lot of possible configurations for electrodes. The simplest one has one cathode and one anode and is thus, with the head tissue as conductor, a full electric circuit. Configurations with a multiset of electrodes provide the possibility to use more complex stimulation protocols.
In this thesis we will consider a more complex electrode setup. The question that arises is what stimulation protocol is optimal for different treatments or experiments with tDCS. A novel work on this topic has been published by Dmochowski et al. [1]2011optimized. In addition we want to mention the PhD-thesis from Sven Wagner [2], where an optimization technique for tDCS was mathematically developed and analysed. Within this thesis we want to compare these different approaches and want to give a guideline in which cases the approaches perform best.

1.2 Structure of the thesis

The thesis is structured as follows:

Chapter 2 gives a short introduction on how a neuron works, and a short introduction to tDCS.

Chapter 3 provides the basic mathematical background which is used in this thesis. It starts with a short introduction of the EEG forward problem and the lead field. Furthermore, it gives an overview of how we formulate convex problems and puts light on the singular value decomposition and the earth mover's distance.

Chapter 4 pictures the general optimization problem we focus on.

Chapter 5 formulates and investigates the different optimization approaches that we use to obtain an optimal tDCS stimulation protocol.

Chapter 6 describes the setup and evaluation of the different simulations we perform. We investigate, based on the humand head model, the performance of the optimization approaches with different predefined targets. Moreover, we will investigate the robustness of the approaches with regards to misspecification of the targets angle. The ferret head model will be used for a simple stimulation, to verify the model. In addition, we take a further look on the approaches based on their behaviour in the ferret head model.

2 Basics

This chapter will give a brief overview about neurological basics and transcranial direct current stimulation.

2.1 Neuron

2.1.1 Physiology of a neuron

A neuron (or nerve cell) is a fundamental part of the human central nervous system. They transmit nerve signals from and to the brain at up to 360 km/h.
We can divide the neuron into 3 subparts: the dendrites, the cell body (or soma) ,and the axon (see figure 2.1). The branching dendrites which pick up signals from other nerve cells, transmit those to the soma. In the soma all the received signals are combined and, under certain conditions, it will generate its own signal (see figure 2.2). This signal will be sent to other nerve or muscle cells through the axon. At the end of the axon there are the axon terminals, which transmit an electro-chemical signal that can stimulate another neuron or another type of cell.

2.1.2 Action potential

In the state where a neuron doesn't receive any signal there is a potential between the intracellular and extracellular domain of approximatively -70 mV. We call this difference the resting membrane potential [4]. The dendrites can change the potential in soma. This is based on an chemical process, which is influenced by the signals they receive from other neurons. If a potential threshold of -55 mV is reached in the soma, the neuron sends down a signal through the axon. After sending this signal the neuron remains in

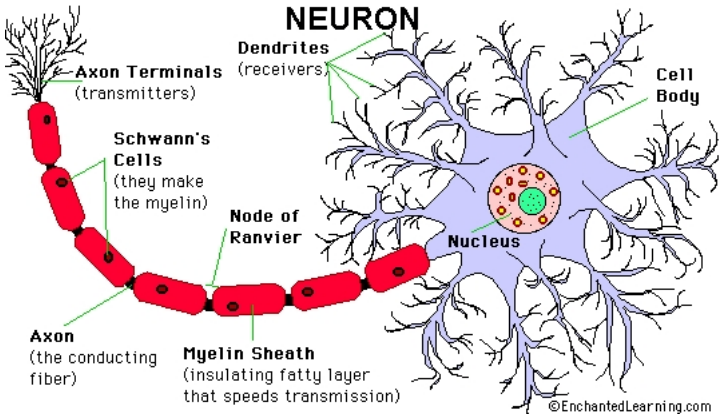

Figure 2.1: Simplified neuron
[3]

a refractory state, which means it doesn't send any signal until it has recovered from this state.

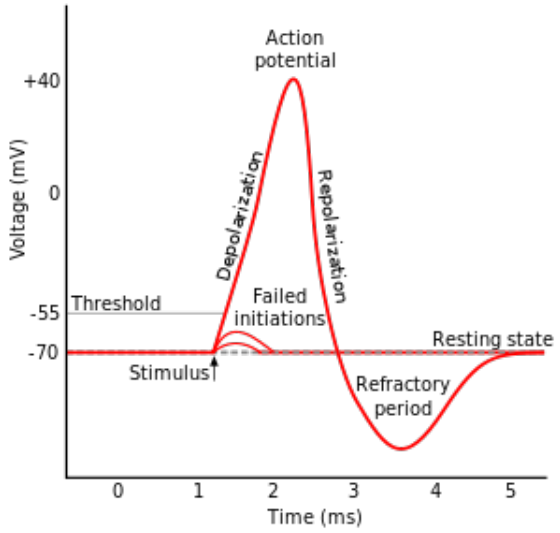

Figure 2.2: Different states of a neuron
[5]

2.2 Transcranial direct current stimulation

The non-invasive technique of tDCS can be manufactured very cheaply and is an easy way to perform brain stimulation. TDCS has been around for over 200 years [6] and was first used on animals. In the last centuries this method was investigated a lot, i.e. [7–9]. Furthermore, to its scientific value, tDCS is also used to treat diseases like depression [10], schizophrenia [11] and Alzheimer's dementia [12]. Another possibility to use tDCS is to enhance cognitive activity like perception [13], attention [14] and

learning [7].

2.3 Basic setup of a tDCS-device

Basically a tDCS-device requires just a few parts, i.e. two electrodes and a battery. With these parts and a conductor like a human head, one can create a circuit.
However, with this small setup one is very limited in case of stimulation. More complex tDCS-devices (see figure 2.3) consists of more than two electrodes, which can be distributed over the conductor and thus allow for a more controlled stimulation.

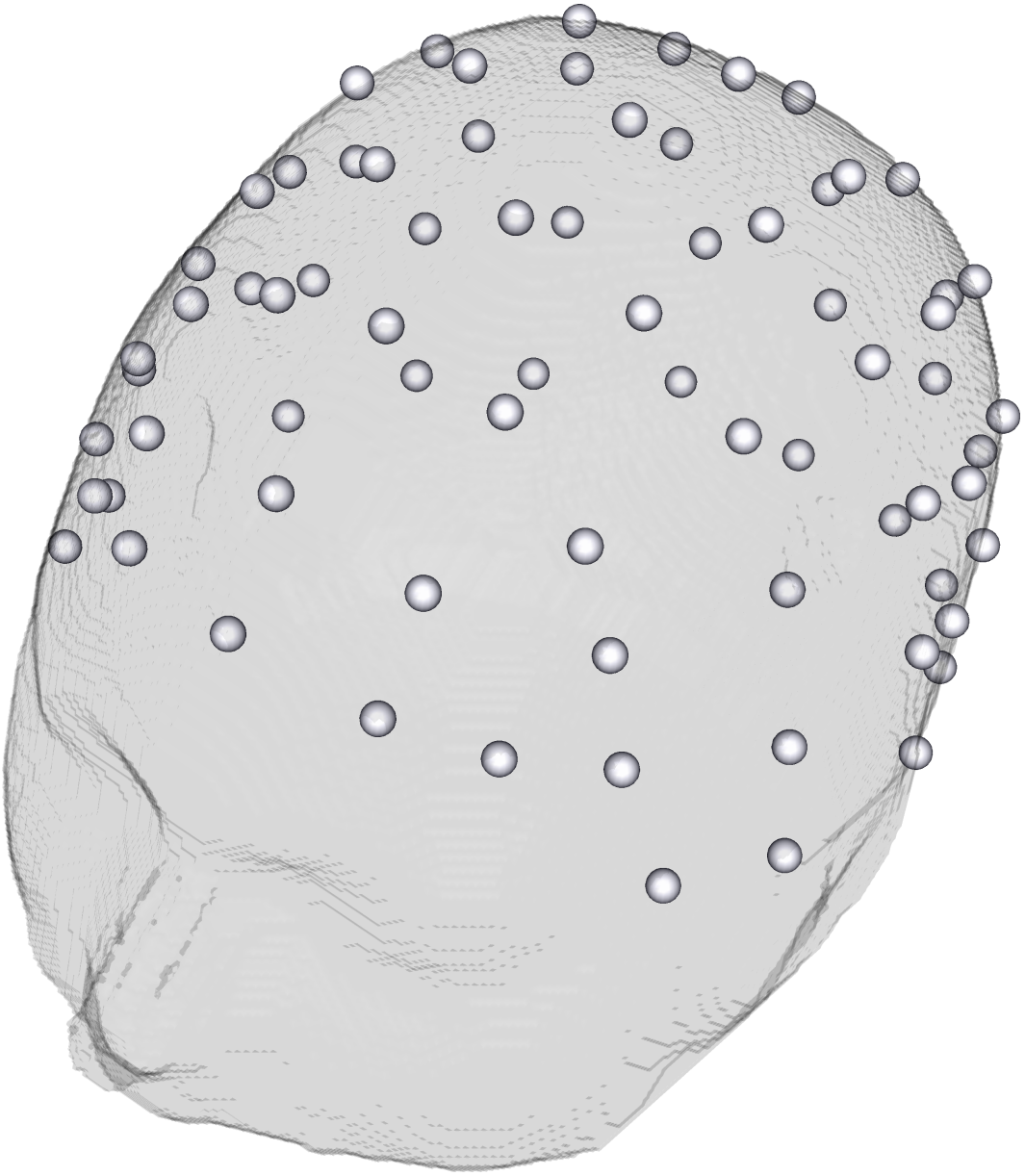

Figure 2.3: Example of a tDCS electrode configuration

2.4 The influence of tDCS on a neuron

With tDCS we are able to influence the firing rate of a neural network. In [15], and [28] was shown that with different directions of stimulation we are able to increase or decrease the amount of spikes a neural network produces. This can cause an alteration of the neural activity in many ways as discussed beforehand.

However, with tDCS we can only use currents below a certain safety constrained, and therefore we only achieve subthreshold stimulation. This means we cannot generate an action potential. However,there are stimulation techniques that can do so, i.e. TMS [16].

3 Mathematical basics

In this chapter we want to provide the mathematical background that we will use in the course of this thesis. We introduce the EEG forward problem and the basic idea of the lead field method. In addition, we discuss the Helmholz' principle of reciprocity and its connection to the lead field theory. Furthermore, we introduce convex problems, singular value decomposition, and the earth mover's distance.

3.1 EEG forward problem

Maxwell equations, which describe a relation between electrical and magnetic fields are crucial for EEG and MEG source analysis. Due to the low-frequency spectrum of EEG/MEG we can use the quasistatic Maxwell equation [17]:

Definition 3.1. Let E be an electric field, B be a magnetic field, μ_0 be the magnetic permittivity and ϵ_0 the electric permittivity. Then the quasistatic formulation of the Maxwell equations is

$$\nabla \cdot E = \frac{\rho}{\epsilon_0}, \tag{3.1}$$

$$\nabla \times E = -\frac{\partial B}{\partial t}, \tag{3.2}$$

$$\nabla \cdot B = 0, \tag{3.3}$$

$$\nabla \times B = \mu_0(j + \epsilon_0 \frac{\partial E}{\partial t}). \tag{3.4}$$

The computation of the electric field follows from

$$E = -\nabla\Phi, \tag{3.5}$$

where Φ is the potential field.
The current density j can be divided into two parts, the primary current density j^p and the secondary current density -$\sigma\nabla \cdot j^p$. Mathematically,that is

$$j := j^p + \sigma E = j^p - \sigma\nabla\Phi. \tag{3.6}$$

Since it is physically realistic, we assume continuous crossings between the boundaries. For the headsurface (Γ) we assume

$$\langle \sigma\nabla\Phi, n\rangle|_\Gamma = 0.$$

Now we use the divergence operator on (3.3), put (3.6) into the resulting formula, and we obtain:

Definition 3.2. The potential equation for the EEG forward problem is given by

$$\nabla \cdot \sigma\nabla\Phi = \nabla \cdot J^p \qquad \text{in } \Omega, \tag{3.7}$$

$$\langle \sigma\nabla\Phi, n\rangle = 0 \qquad \text{on } \partial\Omega\backslash\Gamma_D, \tag{3.8}$$

$$\Phi = 0 \qquad \text{on } \Gamma_D. \tag{3.9}$$

The added homogenous Dirichlet boundary condition ensures a unique solution for the EEG forward problem [2].

Remark 1. The conductivity tensor σ differs between the tissues and as a consequence the boundaries of the tissues have conductivity jumps. Therefore, σ is not in C^1, but in a three dimensional scenario $\sigma \in L^\infty$.

Remark 2. With regards to the previous remark classical the solution is not feasible. Since σ has conductivity jumps at the tissue boundaries, it is discontinues. And as $\sigma\nabla\Phi_{classic}$ is continous in Ω,$\nabla\Phi_{classic}$ has to be discontinues, which leads to $\Phi_{classic} \notin C^1(\Omega)$.

However, a weak solution is given under certain regularity assumptions. If we assume that Ω has a Lipschitz continous boundary, $0 < \sigma \in L^\infty$, and $\nabla J^p \in L^2(\Omega)$, we obtain $\Phi \in H^1(\Omega)$.

3.2 Lead field

We will now introduce a technique which is very useful in EEG/MEG source analysis, the so-called lead field. Once derived, the lead field can be used to compute the forward problems of EEG/MEG multiple times with a little effort. With a discretized formulation of the forward problem we will be able to compute flow fields induced by tDCS.
We will now fix a set of surface electrodes $S = \{s_1, ..., s_l\}$. Let $c \in \mathbb{R}^{3\times 1}$ be the potentials at an arbitrary position $p \in \Omega$, which are generated by a unit vector parallel to the x,y,z axis, respectivly. To get an estimation of the potential vector c, we have to solve the EEG forward problem for every direction once. With a given dipole position p and its moment q we can easily calculate the potential field

$$\Phi(p) = \langle c, q \rangle. \tag{3.10}$$

Definition 3.3. Let $\Phi(s_i)$ and $\Phi(s_i)$ be the potentials at electrode locations s_i and s_j generated by a dipole at x_0 with moment q. c_{s_i} and c_{s_j} are the potentials alongside the cartesian axis, respectively. 3.10 now allows us to easily calcutate the potential difference

$$\Phi(s_i) - \Phi(s_j) = \langle c_{s_i}, q \rangle - \langle c_{s_j}, q \rangle = \langle c_{s_i} - c_{s_j}, q \rangle := \langle l_{s_i s_j}, q \rangle$$

between the surface electrodes.
We name $l_{s_i s_j}$ the lead vector. If we compute the lead vector for every element in the source space we obtain the so-called lead field vector $L_{i,j} \in \mathbb{R}^{3M}$, where M is the amount of source space nodes.

Definition 3.4. Let $L_{i,j} \in \mathbb{R}^{3M}$ be the lead field vector according to the electrodes $s_i s_j$. The so-called lead field matrix L can now be obtained by fixing the first electrode as reference, calculating the lead field vectors $L_{2,1}, ..., L_{l,1}$ and defining L := $[L_{2,1}, ..., L_{l,1}]$.

3.3 Helmholtz' principle of reciprocity

In the following section we will introduce Helmholtz' principle of reciprocity. This will provide a technique to calculate the lead field matrix from a sensor point view, which we exploit for tDCS simulation and optimization.

Theorem 1. (Helmholtz' principle of reciprocity) In a volume conductor model a source at a given position p_{source} and a sink at a given position p_{sink} are generating a source

$$I = I^*\delta(p_{source} - x_0) - I^*\delta(p_{sink} - x_0)$$

In addition, a current density J is introduced at p_{in} and removed at p_{out} on the boundary of the volume conductor $\partial\Omega$

$$J = J^*\delta(p_{in} - x_0) - J^*\delta(p_{out} - x_0).$$

Then

$$I^*[\Phi_2(p_{source}) - \Phi_2(p_{sink})] = J^*[\Phi_1(p_{in}) - \Phi_1(p_{out})]$$

holds, where Φ_1 and Φ_2 being the potential field generated by the volume current source I and the surface density J, respectively.

Proof. see [2] □

3.4 Calculating lead field via reciprocity

Let Ω be a volume conductor with a fixed pair of electrodes. Currents injected with one electrode and withdrawn with the other generate a reciprocal potential field Φ_{rec}. Thus the electric field is given by $E_{rec} = -\nabla\Phi_{rec}$ and the current density field is given by $J_{rec} = \sigma E_{rec}$.

Lemma 1. Let Φ_{rec} be the reciprocal potential field and let us consider a current source and sink generating a current dipole with strength I^*. In addition, let q be a dipole moment that is orientated from source to sink

$$q = I(p_{source} - p_{sink}). \tag{3.11}$$

Then

$$I(\Phi_{rec}(p_{source}) - \Phi_{rec}(p_{sink}) = \langle\nabla\Phi_{rec}(p_{source}), q\rangle \tag{3.12}$$

holds.

Proof. see [2] □

The following theorem will describe the relation between Φ and Φ_{rec}.

Theorem 2. Let $\Phi_{in,out} = \Phi(p_{in}) - \Phi(p_{out})$ be the potential difference at the surface electrodes. Then

$$\Phi_{in,out} = \langle -\nabla \Phi_{rec}(p_{source}), q \rangle \tag{3.13}$$

holds.

Proof. see [2] □

The last theorem shows that we are not only able to compute the lead field matrix from a source point of view, but from a sensor point of view as well.

3.5 Convex problems

In this section we will give a brief overview about convex problems. The following section is based on [18]. For further reading we recommend that script.

3.5.1 Basic terminology

The following formulation

$$\begin{aligned} &\text{minimize } f_0(x) \\ &\text{subject to } f_i(x) \leq 0, f_i(x) \quad i = 1, ..., m \\ &\qquad\qquad h_j(x) = 0, \qquad\quad j = 1, ...p \end{aligned} \tag{3.14}$$

describes the problem of finding an x that minimizes f_0 and also fulfils the constraints $f_i(x) \leq 0$ for i=1,...,p, and $h_j(x) = 0$ for j=1,...,p. We call $x \in \mathbb{R}^n$ the optimization variable and $f_0(x) : \mathbb{R}^n \to \mathbb{R}$ is called the cost function. The inequalities $f_i(x) \leq 0$ are called inequality constraints and the equalities $h_j(x) = 0$ are called equality constraints. Analogously we call the functions $f_i : \mathbb{R}^n \to \mathbb{R}$ and $h_j : \mathbb{R}^n \to \mathbb{R}$ inequality and equality constraint functions.
We call a point p feasible, if it satisfies the constraints of the problem. Furthermore we call a problem feasible if it has at least one feasible point. Otherwise we call it infeasible.

$$p^* = inf\{f_0(x) \mid f_i(x) \leq 0 \text{ for } i = 1, ..., m \text{ and } h_i(x) = 0 \text{ for } i = 1, ..., p\} \tag{3.15}$$

is called the optimal value of the problem 3.14. In case of $p^* = \infty$, we call it an infeasible problem. If there is a sequence of feasible points $(x_k)_k$ with $f_0(x_k) \to -\infty$, then $p^* = -\infty$ and we call (3.14) unbounded below.

3.6 Singular value decomposition

Let $A \in \mathbb{R}^{m \times n}$. Then there exist orthogonal matrices $U \in \mathbb{R}^{m \times m}$ and $V \in \mathbb{R}^{n \times n}$ such that

$$U^T AV = \Sigma = diag(\sigma_1, ..., \sigma_p),$$

where $p = min(m, n)$ and $\sigma_1 \leq \sigma_2 \leq ... \leq \sigma_p \leq 0$.

Proof. see [19] □

3.7 Earth mover's distance

We will now introduce the earth mover's distance (EMD) based on [20].
The EMD is a measure of distance between two normalized distributions over a given region. It provides an indicator of the similarity of different distributions. To give a visual explanation, imagine two piles of sand. The EMD gives the minimum cost of turning the one pile into the other.
Let $P = \{(p_1, w_{p_1}), ..., (p_m, w_{p_m})\}$ be a signature with m cluster, p_i the representative, and w_{p_i} the weight of the cluster, analoguesly let $Q = \{(q_1, w_{q_1}, ..., (q_n, w_{q_n})\}$ be. Let $D = (d_{ij})_{ij}$ be the ground distance between the cluster p_i and q_j.
We are looking for a flow matrix $F = (f_{ij})_{ij}$, where f_{ij} describes the flow between p_i and q_j, that minimizes a given cost function.
This leads to the following formulation:

$$\text{minimize } f(F) = \sum_{i=1}^{m} \sum_{j=1}^{n} d_{ij} f_{ij},$$

$$\text{subject to } f_{ij} \geq 0 \qquad 1 \leq i \leq m, 1 \leq j \leq n, \tag{3.16}$$

$$\sum_{j=1}^{n} f_{ij} \leq w_{p_i} \qquad 1 \leq i \leq m, \tag{3.17}$$

$$\sum_{i=1}^{m} f_{ij} \leq w_{q_j} \qquad 1 \leq j \leq n, \tag{3.18}$$

$$\sum_{i=1}^{m}\sum_{j=1}^{n} f_{ij} = min(\sum_{i=1}^{m} w_{p_i}, \sum_{j=1}^{n} w_{q_j}). \tag{3.19}$$

Now we can compute the

$$EMD = \frac{\sum_{i=1}^{m}\sum_{j=1}^{n} d_{ij} f_{ij}}{\sum_{i=1}^{m}\sum_{j=1}^{n} f_{ij}}$$

4 General problem

In this chapter we describe the tDCS optimization problem. It is based on paper [1]. For further information we highly recommend reading it.

In tDCS we try to stimulate regions in the brain through direct currents. These currents are injected by given electrodes which are distributed over the head, e.g. the 10-20 or 10-10 EEG electrode set up. The optimal stimulation protocol highly depends on different factors, e.g. the target (orientation, location), positions of the electrode, and the head model. A stimulation experiment may have different requirements on the stimulation. Some may need high current density at the target, others need high focality, and others need a precise orientation of the stimulus. These constraints may need different optimization approaches to achieve an optimal stimulation protocol.

We will provide a forward model of the current flow, which are similar to the models used to solve EEG inverse problems. We will use this forward model to optimize stimulation to obtain a desired electric field.

A head has different tissues with different kind of conductivities. These tissues are not isotropic and this leads to a very complex volume conductors. In the different tissues there are neither sources nor sinks in the different tissues, thus the current density J can be described by the Laplace equation

$$\nabla J = 0.$$

In tDCS we apply current at the surface electrodes. Therefore, if we want to compute the resulting potential distribution Φ, we can use the modified Laplace equation

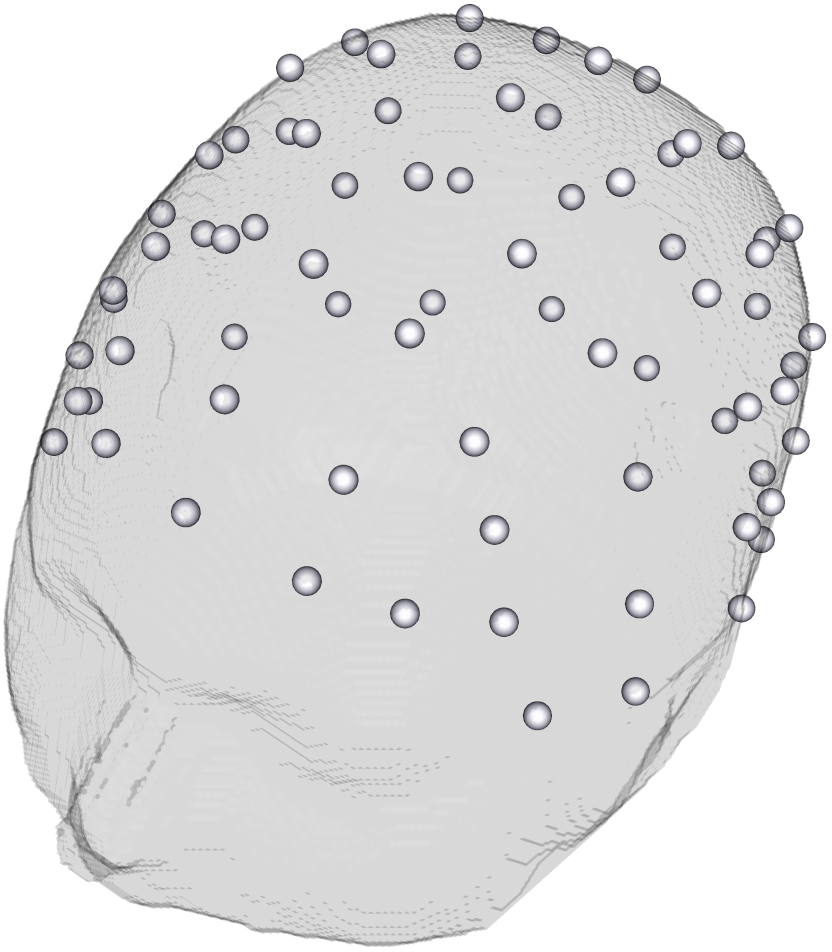

Figure 4.1: 10-10 system Electrode setup

$$\nabla J = (\sigma E) = \nabla(-\sigma \nabla \Phi) = 0.$$

Under certain assumptions we can find a unique solution [2], however, in general this approach doesn't hold. Therefore, we may find a numerical solution through discretisation of the volume conductor into a set of finite elements. In our set up we have the electrodes which inject a given current density at the surface of our volume conductor. The rest of the outer boundary can thus be set to zero.

Let M be the number of electrodes and add a reference electrode to this setup. We assume M different boundary conditions. The mth boundary condition will be denoted as $\mathbb{B}_m$. So under the condition $\mathbb{B}_m$, the boundary is zero everywhere, except at the mth electrode and the reference electrode. These two electrodes will act as cathode and anode (doesn't matter which way we choose cathode/anode, but it has to be the same in all boundary conditions). For each boundary condition we compute the lead field matrix to obtain the effective resistivity $a_m \in \mathbb{R}^3$. The effective resistivity

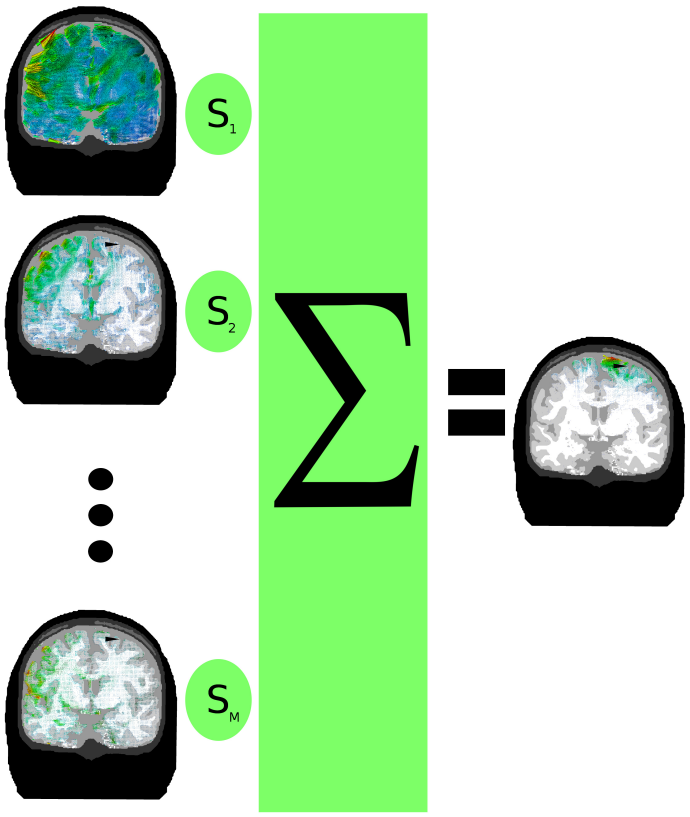

Figure 4.2: Visualization of influence matrix

describes the quantity of the magnitude of applied current to the induced electric field. In other words, we can compute the electric field vector $e_m \in \mathbb{R}^3$ at a certain position $r_n \in \mathbb{R}^3, n \in \{1, ..N\}$, where N is the amount of FEM nodes, through

$$e_m(r_n) = s_m a_m(r_n),$$

where s_m is the applied current density.

We now consider a situation where we stimulate through more than one electrode. Due to the linearity of the Laplace equation we can easily compute the electric field

$$e(r_n) = \sum_{m=1}^{M} e_m(r_n) = \sum_{m=1}^{M} s_m a_m(r_n).$$

In addition, we can rewrite this in matrix form

$$e = As$$

where

$$e = \begin{bmatrix} e(r_1) \\ e(r_2) \\ \vdots \\ e(r_N) \end{bmatrix}, A = \begin{bmatrix} a_1(r_1) & \cdots & a_m(r_1) \\ \vdots & & \vdots \\ a_1(r_N) & \cdots & a_m(r_N) \end{bmatrix}, s = \begin{bmatrix} s_1 \\ s_2 \\ \vdots \\ s_m \end{bmatrix}.$$

The optimization problem we have to solve is to find the right s. For this we have M degrees of freedom because we can choose the current density at the M electrodes. To avoid loading or deloading of the head the electrode that has been used as reference electrode is set to $-\sum_m s_m$, so that the sum of all electrodes is zero. How the optimization for the current applied at the electrodes can be carried out is part of the next chapter.

5 Optimization

Finding an optimal stimulation is a crucial part of brain stimulation. Certain experiments require different set-ups of the hardware and thus leading to different optimization problems. In this chapter we want to focus on techniques that can be used for tDCS stimulation protocol optimization.

5.1 Alternating direction method of multipliers

This section introduces the alternating direction method of multipliers (ADMM). We will do this step by step. First we will discuss the dual ascent, then the dual decomposition, augmented Lagrangians and the method of multipliers. Finally we will put the previous mentioned methods together to get the basic idea of ADMM. The following section refers directly to [21].

5.1.1 Dual ascent

We will look at a simple equality-constrained convex optimization problem

$$\begin{aligned} &\text{minimize} f(x), \\ &\text{subject to } Ax = b, \end{aligned} \tag{5.1}$$

where $x \in \mathbb{R}^n$, $A \in \mathbb{R}^{m \times n}$ and $f : \mathbb{R}^n \to \mathbb{R}$ is a convex function
Thus we can write the Lagrangian of 5.1 as

$$L(x, y) = f(x) + y^T(Ax - b).$$

Furthermore, we define the so called dual function as

$$g(y) = \inf_x L(x, y) = -f^*(-A^T y) - b^T y,$$

And we call

$$\max_y g(y)$$

the dual problem.
The dual ascent method uses the gradient ascent to solve the dual problem. Under the assumption that g is differentiable following iteration

$$x^{k+1} := \operatorname{argmin}_x L(x, y^k),$$
$$y^{k+1} := y^k + \alpha^k (Ax^{k+1} - b),$$

solves the problem, where α^k is the step size. The interesting part of this algorithm is the y-update. It can be seen as a price update we have to pay for every iteration step. Thus the dual function increases in every step.

5.1.2 Dual decomposition

Now we want to introduce a method that can improve the dual ascent in terms of computation speed. If

$$f(x) = \sum_{i=1}^{N} f_i(x_i), \tag{5.2}$$

is fulfilled,where $x = (x_1,...,x_N)$ and $x_i \in \mathbb{R}^{n_i}$ are subvectors of x, it is possible to alternate the iterations Furthermore the Matrix $A = (A_1,...A_N)$ is partitioned so $Ax = \sum_{i=1}^{N} A_i x_i$. In addition we write the Lagrangian as

$$L(x, y) = \sum_{i=1}^{N} L_i(x_i, y) = \sum_{i=1}^{N} (f_i(x_i) + y^T A_i x_i - (1/N) y^T b). \tag{5.3}$$

So if we reconsider the dual ascent, we can use the algorithm

$$x_i^{k+1} := \operatorname{argmin}_{x_i} L_i(x_i, y^k), \tag{5.4}$$
$$y^{k+1} := y^k + \alpha^k (Ax^{k+1} - b) \tag{5.5}$$

to solve the decomposed problem. The main advantage is that we can solve the N problems for the x-minimization step parallel. However the cost we have to pay is the effort of distributing the N x_i-minimization problems on the different processors. Also after this step we have to merge the x_i together for the y-update.

5.1.3 Augmented Lagrangians and the method of multipliers

In this section we improve the dual ascent in terms of robustness and convergence. The augmented Lagrangians for 3.14 is

$$L_p(x, y) = f(x) + y^T(Ax - b) + (\rho/2)\,\|Ax - b\|_2^2 \tag{5.6}$$

with a penalty parameter ρ.
The augmented Lagrangians is the classic Lagrangians for the problem

$$\begin{aligned} &\text{minimize } f(x) + (\rho/2)\,\|Ax - b\|_2^2 \\ &\text{subject to } Ax = b \end{aligned} \tag{5.7}$$

It is easy to see that 5.7 and 5.1 are equivalent problems, since for all feasible points the constraint $Ax = b$ implies $\|Ax - b\|_2^2 = 0$. $g_\rho = \underset{x}{\operatorname{argmin}}\ L_\rho(x, y)$ is the dual function for 5.7 and is differentiable under far less assumptions than the dual function of 5.1.
To solve 5.7 we will also make use of the ascent gradient method in terms of dual ascent

$$x^{k+1} := \underset{x}{\operatorname{argmin}}\ L_\rho(x, y^k), \tag{5.8}$$

$$y^{k+1} := y^k + \rho(Ax^{k+1} - b). \tag{5.9}$$

We call this "method of multipliers" for solving 3.14. A different Lagrangian and the step size α_k was subsidized by the penalty parameter ρ.

5.1.4 ADMM-Algorithm

The next algorithm we will present tries to combine the decomposability of dual ascent and the superior convergence of the method of multipliers. Problems solved by ADMM have the form

$$\begin{aligned} &\text{minimize } f(x) + g(x) \\ &\text{subject to } Ax + Bz = c \end{aligned} \tag{5.10}$$

where $x \in \mathbb{R}^n$, $z \in \mathbb{R}^m$, $A \in \mathbb{R}^{p\times n}$, $B \in \mathbb{R}^{p\times m}$, and $C \in \mathbb{R}^p$.

This leads to the augmented Lagrangian

$$L_\rho(x, y, z) = f(x) + g(z) + y^T(Ax + Bz - c) + (\rho/2)\,\|Ax + Bz - c\|_2^2\,. \tag{5.11}$$

Thus with the method of multiplier we obtain

$$(x^{k+1}, z^{k+1}) := \underset{x,z}{\operatorname{argmin}}\ L_\rho(x, y^k, z), \tag{5.12}$$

$$y^{k+1} := y^k + \rho(Ax^{k+1} + Bz^{k+1} - c). \tag{5.13}$$

In this case we minimize the two primal variables jointly. However in the ADMM case we use following iteration

$$x^{k+1} := \underset{x}{\operatorname{argmin}}\ L_\rho(x, y^k, z^k), \tag{5.14}$$

$$z^{k+1} := \underset{z}{\operatorname{argmin}}\ L_\rho(x^{k+1}, y^k, z), \tag{5.15}$$

$$y^{k+1} := y^k + \rho(Ax^{k+1} + Bz^{k+1} - c). \tag{5.16}$$

So the ADMM does not minimize the two dual variables at the same time. Due to sequential computation of these two dual variables we add the term alternating direction to the method of multipliers. It is nearly the same as the method of multipliers, but instead of jointly minimizing, we use a Gauss-Seidel step for each dual variable. Another advantage of this separation of x and z is that we are now able to use the decomposition approach if f or g are separable. It is also worth mentioning that one can exchange the update order of x and z. As in the above case in a step $k+1$ the z^{k+1} update depends and the x^{k+1} update, the iteration could behave differently with a different order of updates. Additionally, one can easily extend this algorithm with more dual variables.

5.1.5 Convergence of ADMM

For analysing the convergence we make two assumptions.

Assumption 1. The functions $f : \mathbb{R}^n \to \mathbb{R} \cup \infty$ and $g : \mathbb{R}^n \to \mathbb{R} \cup \infty$ are closed, proper, and convex.

This assumption can also be expressed with the epigraph of f and g.
A function $f : \mathbb{R}^n \to \mathbb{R} \cup \infty$ is closed, proper and convex if and only if

$$epi f = \{(x, t) \in \mathbb{R}^n \times \mathbb{R} | f(x) \leq t\} \tag{5.17}$$

is a closed convex set.

Assumption 2. The augmented Lagrangian L_0 has a saddle point. In other words there exists (x^*,z^*,y^*) where

$$L_0(x^*, z^*, y) \leq L_0(x^*, z^*, y^*) \leq L_0(x, z, y^*) \tag{5.18}$$

holds for all x, z, y.

These assumptions allow us to show following convergence statements:

1. Residual convergence: $r^k = Ax^k + Bz^k - c \to 0$ as $k \to \infty$
2. Objective convergence: $p^k = f(x^k) + g(x^k) \to f(x^*) + g(x^*) = p^*$ as $k \to \infty$
3. Dual variable convergence: $y^k \to y^*$ as k $\to \infty$

Proof. First of all we will show the inequalities

$$p^* - p^{k+1} \leq y^{*T} r^{k+1}, \tag{5.19}$$
$$p^{k+1} - p^* \leq -(y^{k+1})^T r^{k+1} - \rho(B(z^{k+1} - z^k))^T(-r^{k+1} + B(z^{k+1} - z^*)), \tag{5.20}$$
$$V^{k+1} \leq V^k - \rho \left\|r^{k+1}\right\|_2^2 - \rho \left\|B(z^{k+1} - z^k)\right\|_2^2 \tag{5.21}$$

where

$$V^k = (1/\rho) \left\|y^k - y^*\right\|_2^2 + \rho \left\|B(z^k - z^*)\right\|_2^2. \tag{5.22}$$

Assumption 2 provides the inequality

$$\begin{aligned} p^* &= f(x^*) + g(z^*) \\ &= f(x^*) + g(z^*) + (y^*)^T(Ax^* + Bz^* - c) \\ &= L_0(x^*, z^*, y^*) \\ &\leq L_0(x^{k+1}, z^{k+1}, y^*) \\ &= f(x^{k+1}) + g(x^{k+1}) + (y^*)^T r^{k+1} \\ &= p^{k+1} + (y^{*T})r^{k+1} \end{aligned}$$

and thus 5.19 is shown.
Since x^{k+1} is a minimizer of $L_\rho(x, z^k, y^k)$, the optimal condition is
$0 \in \frac{\partial}{\partial x} L_\rho(x^{k+1}, z^k, y^k) = \frac{\partial}{\partial x} f(x^{k+1}) + A^T y^k + \rho A^T(Ax^{k+1} + Bz^k - c)$.
Furthermore, we make use of the relation $y^{k+1} = y^k + \rho r^{k+1}$ and rearrange it to

$y^k = y^{k+1} - \rho r^{k+1}$. Thus it is
$0 \in \frac{\partial}{\partial x} f(x^{k+1}) + A^T(y^{k+1} - \rho B(z^{k+1} - z^k))$.
Therefore, x^{k+1} minimizes $f(x) + (y^{k+1} - \rho B(z^{k+1} - z^k))^T Ax$.

Also z^{k+1} is a minimizer of $L_\rho(x^k, z, y^k)$ and thus we obtain the optimality condition
$0 \in \frac{\partial}{\partial z} L_\rho(x^k, z^{k+1}, y^k) = \partial g(z^{k+1}) + B^T y^k + \rho B^T(Ax^k + Bz^{k+1} - c)$.
With the previous relation of y^k and y^{k+1} we obtain
$0 \in \frac{\partial}{\partial x} g(z^{k+1}) + B^T y^{k+1}$
Consequently z^{k+1} minimizes $g(z) + y^{(k+1)T} Bz$.

This leads to the inequalities

$$\begin{aligned} f(x^{k+1}) + (y^{k+1} - \rho B(z^{k+1} - z^k))^T Ax^{k+1} \leq \quad & f(x^*) + (y^{k+1} - \rho B(z^{k+1} - z^k))^T Ax^* \\ g(z^{k+1}) + y^{(k+1)T} Bz^{k+1} \leq \quad & g(z^*) + y^{(k+1)T} Bz^*. \end{aligned}$$

With these equalities we can show

$$\begin{aligned} p^{k+1} - p^* =& f(x^{k+1}) + g(z^{k+1}) - f(x^*) - g(x^*) \\ \leq& (y^{k+1} - \rho B(z^{k+1} - z^k))^T Ax^* \\ & - (y^{k+1} - \rho B(z^{k+1} - z^k))^T Ax^{k+1} \\ & + (y^{k+1})^T B(z^* - z^{k+1}) \\ =& - (y^{k+1})^T (Ax^{k+1} + Bz^{k+1} - c) \\ & + (y^{k+1})^T (Ax^* + Bz^* - c) \\ & + \rho(B(z^{k+1} - z^k)^T)(Ax^{k+1} - Ax^*) \\ =& - (y^{k+1})^T r^{k+1} + \rho(B(z^{k+1} - z^k)^T (r^{k+1} + B(z^{k+1} - z^*)) \end{aligned}$$

and thus (5.20) is shown.

Now we will add (5.19) and (5.20) together, multiply it by 2, and rearrange the terms, hence

$$\begin{aligned} 0 &\geq y^{*T} r^{k+1} - (y^{k+1})^T r^{k+1} - \rho(B(z^{k+1} - z^k))^T(-r^{k+1} + B(z^{k+1} - z^*)) \\ &= 2(y^{k+1} - y^*)^T r^{k+1} - 2\rho(B(z^{k+1} - z^k))^T r^{k+1} + 2\rho(B(z^{k+1} - z^k))^T(B(z^{k+1} - z^*)). \end{aligned}$$

In the next step we will rewrite the last part of the upper equation. First we will substitute $y^{k+1} = y^k + \rho r^{k+1}$,so we get

$$\begin{aligned}2(y^{k+1}-y^*)^T r^{k+1} &= 2(y^k-y^*)^T r^{k+1} + \rho\left\|r^{k+1}\right\|_2^2 + +\rho\left\|r^{k+1}\right\|_2^2 \\ &= \frac{2}{\rho}(y^k-y^*)^T(y^{k+1}-y^k) + \frac{1}{\rho}\left\|y^{k+1}-y^k\right\|_2^2 + \rho\left\|r^{k+1}\right\|_2^2 \\ &= \frac{1}{\rho}(\left\|y^{k+1}-y^*\right\|_2^2 - \left\|y^k-y^*\right\|_2^2) + \rho\left\|r^{k+1}\right\|_2^2\end{aligned}$$

In addition, we can write

$$\begin{aligned}&\rho\left\|r^{k+1}\right\|_2^2 - 2\rho(B(z^{k+1}-z^k))^T r^{k+1} + 2\rho(B(z^{k+1}-z^k))^T(B(z^{k+1}-z^*)) \\ =&\rho\left\|r^{k+1}\right\|_2^2 - 2\rho(B(z^{k+1}-z^k))^T r^{k+1} + 2\rho(B(z^{k+1}-z^k))^T(B((z^{k+1}-z^k)+(z^k-z^*)) \\ =&\rho\left\|r^{k+1}\right\|_2^2 - 2\rho(B(z^{k+1}-z^k))^T r^{k+1} + 2\rho\left\|B(z^{k+1}-z^k)\right\|_2^2 + 2\rho(B(z^{k+1}-z^k)^T - B(z^k-z^*)) \\ =&\rho\left\|r^{k+1}+B(z^{k+1}-z^k)\right\|_2^2 + \rho\left\|B(z^{k+1}-z^k)\right\|_2^2 + 2\rho(B(z^{k+1}-z^k)^T - B(z^k-z^*)) \\ =&\rho\left\|r^{k+1}+B(z^{k+1}-z^k)\right\|_2^2 + \rho\left\|B((z^{k+1}-z^*)+(z^*-z^k))\right\|_2^2 + 2\rho(B(z^{k+1}-z^k)^T - B(z^k-z^*)) \\ =&\rho\left\|r^{k+1}+B(z^{k+1}-z^k)\right\|_2^2 + \rho\left\|B(z^{k+1}-z^*)\right\|_2^2 + \rho\left\|B(z^*-z^k)\right\|_2^2.\end{aligned}$$

Taking all the results together, we obtain

$$\begin{aligned}0 \geq \frac{1}{\rho}(\left\|y^{k+1}-y^*\right\|_2^2 - \left\|y^k-y^*\right\|_2^2) + \rho\left\|r^{k+1}+B(z^{k+1}-z^k)\right\|_2^2 + \rho\left\|B(z^{k+1}-z^*)\right\|_2^2 \\ + \rho\left\|B(z^k-z^*)\right\|_2^2.\end{aligned}$$

which provides

$$\begin{aligned}V^k - V^{k+1} &\geq \rho\left\|r^{k+1}+B(z^{k+1}-z^k)\right\|_2^2 \\ &= \rho\left\|r^{k+1}\right\|_2^2 + 2\rho r^{k+1}B(z^{k+1}-z^k) + \rho\left\|z^{k+1}-z^k\right\|_2^2\end{aligned}$$

Furthermore, we need to show

$$2\rho r^{k+1}B(z^{k+1}-z^k) \geq 0. \tag{5.23}$$

Remember that z^{k+1} minimizes $g(z) + y^{(k+1)T}Bz$ and z^k minimizes $g(z) + y^{kT}Bz$. Now

we can combine

$$g(z^{k+1}) + y^{(k+1)T} B z^{k+1} \leq g(z^k) + (y^{k+1})^T B z^k$$

and

$$g(z^k) + y^{(k)T} B z^k \leq g(z^{k+1}) + y^{(k)T} B z^{k+1}$$

to get

$$\begin{aligned} 0 &\geq (y^{k+1} - y^k)^T (B(z^{k+1} - z^k)) \\ &= \rho(r^{(k+1)T})(B(z^{k+1} - z^k)). \end{aligned}$$

Since ρ is non-negative we have shown 5.23.

Since $\left\|r^{k+1}\right\|_2^2$ and $\left\|(z^{k+1} - z^k)\right\|_2^2$ are positive and $V^k \leq V^0$ by 5.21 it follows that y^k and Bz^k are bounded.

No we can sum up the V^k

$$\sum_{k=0}^{\infty} V^k = \rho(\sum_{k=0}^{\infty} \left\|r^{k+1}\right\|_2^2 + \left\|z^{k+1} - z^k\right\|_2^2) \leq V_0,$$

which implies $\left\|z^{k+1} - z^k\right\|_2^2$ and $\left\|r^{k+1}\right\|_2^2 \to 0$ for $k \to \infty$. So the residual convergence 5.19 and dual variable convergence5.21 is shown.

As y^k is bound and r^k $B(z^{k+1} - z^k)$ converges to zero, we can conclude from 5.19 and 5.21 the objective convergence.

□

5.2 Linearly constrained minimum variance

In this section section we will discuss another optimization problem called "Linearly Constrained Minimum Variance" (LCMV). This approach is especially interesting as it focuses on optimizing a vector at a specific location.

$$\begin{aligned} &\text{minimize } f(x) \\ &\text{subject to } Cx = e \end{aligned} \tag{5.24}$$

where $f(x) = \|Ax\|_2^2$, $x \in \mathbb{R}^m$, $A \in \mathbb{R}^{n \times m}$ with full rank, $C(i) = [a_{i1} a_{i2} \cdots a_{im}] \neq 0$, and $e \in \mathbb{R}^n$.

Theorem 3. The solution to (5.24) is

$$(A^T A)^{-1} C [C^T (A^T A)^{-1} C]^{-1} e.$$

Proof. First we will define the Lagrangian

$$L(x) = \frac{1}{2} f(x) + \lambda^T (C^T x - e).$$

Taking the gradient of L and set it equal 0, we obtain

$$A^T A x + C\lambda = 0.$$

Thus

$$x_{opt} = -(A^T A)^{-1} C\lambda$$

is an optimal.
Since e has to satisfy the constrained of 6.3

$$e = C^T x_{opt} = -C^T (A^T A)^{-1} C\lambda$$

As $(A^T A)^{-1}$ is positive definite $[C^T (A^T A)^{-1} C]^{-1}$ exists and thus the Lagrangian multiplier is

$$\lambda = -[C^T (A^T A)^{-1} C]^{-1} e.$$

All in all we get

$$x_{opt} = (A^T A)^{-1} C[C^T (A^T A)^{-1} C]^{-1} e.$$

□

5.3 Maximal intensity

The maximal intensity approach tries to reach a value e at a predefined point under a certain constraint. This approach is similar to the LCMV approach as it focuses on optimizing a certain vector at a specific location. However, the overall vectorfield is not minimized.

$$\begin{aligned} \text{maximize } & f(x) = e^T C x \\ \text{subject to } & h(x) \leq a \\ & g(x) = b \end{aligned} \tag{5.25}$$

where C is defined as in (5.24).

5.4 Least square

The least-square method is a well known and easy to compute approach to optimization problems.

5.4.1 Unweighted least square

The problem is to

$$\text{minimize } \|Ax - e\|_2^2 \tag{5.26}$$

where $x \in \mathbb{R}^m$ $A \in \mathbb{R}^{n \times m}$ with full rank, $e \in \mathbb{R}^n$
and the solution can be easily computed by

$$x_{opt} = (A^T A)^{-1} A^T e. \tag{5.27}$$

5.4.2 Weighted least square

$$\text{minimize } \|W(Ax-e)\|_2^2 \tag{5.28}$$

where $x \in \mathbb{R}^m$ $A \in \mathbb{R}^{n\times m}$ and invertible, $W \in \mathbb{R}^{n\times n}$, $e \in \mathbb{R}^n$,
and the solution can easily computed by

$$x_{opt} = [(WA)^T WA]^{-1}(WA)^T We \tag{5.29}$$

5.4.3 Least square and SVD

Th singular value decomposition from section 3.6 will now be used to reformulate 5.26. A matrix $A \in \mathbb{R}^{n\times m}$ can be rewritten as

$$A = U\Sigma V^T$$

with $U \in \mathbb{R}^{n\times m}$, $V \in \mathbb{R}^{m\times m}$ being unitary, and $\Sigma \in \mathbb{R}^{m\times m}$ being diagonal. Thus we can reformulate 5.26 to

$$\begin{aligned} &\|Ax-e\|_2^2 \\ =&\left\|U\Sigma V^T x-e\right\|_2^2 \\ =&\left\|\Sigma V^T x-U^T e\right\|_2^2. \end{aligned}$$

With this formulation the dimension of the problem is now equal the number of electrodes m, which is far less than the amount of nodes n, which leads to faster computation.

6 Simulation: Human

In this chapter we want to simulate tDCS. For this we will provide a FE head models that will be used for simulation and optimization. This is a highly-realistic geometry-adapted hexahedral FE 6-compartment human head model with white matter anisotropy.

6.1 Human head model

In this section we want to provide a broad overview of the highly-realistic geometry-adapted hexahedral FE 6-compartment human head model. For further reading we suggest [22].

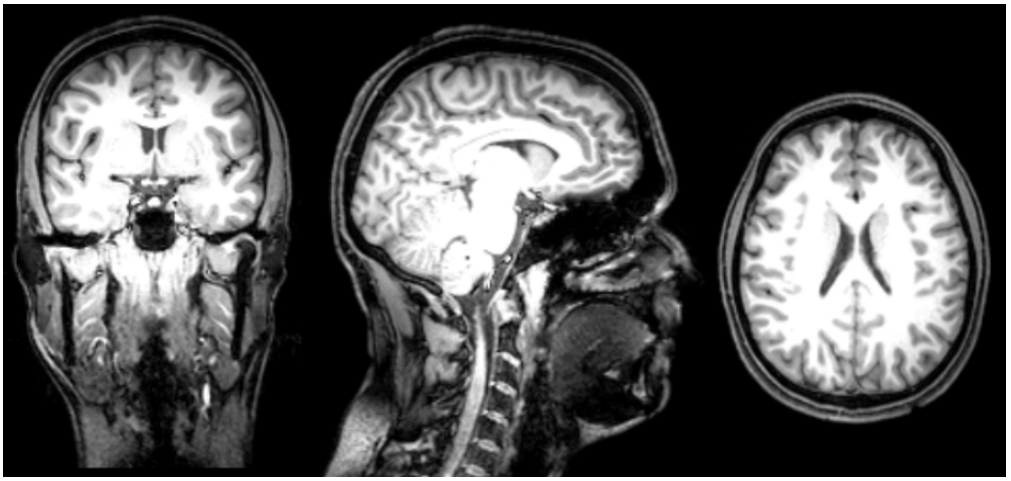

Figure 6.1: T1-weighted human MRI
Sagittal(left), coronal (middle) and axial (right) slice of a T1-image.

First of all we acquire the T1w-, T2w- and DW-MRI (compare figure 6.1 and 6.2). With

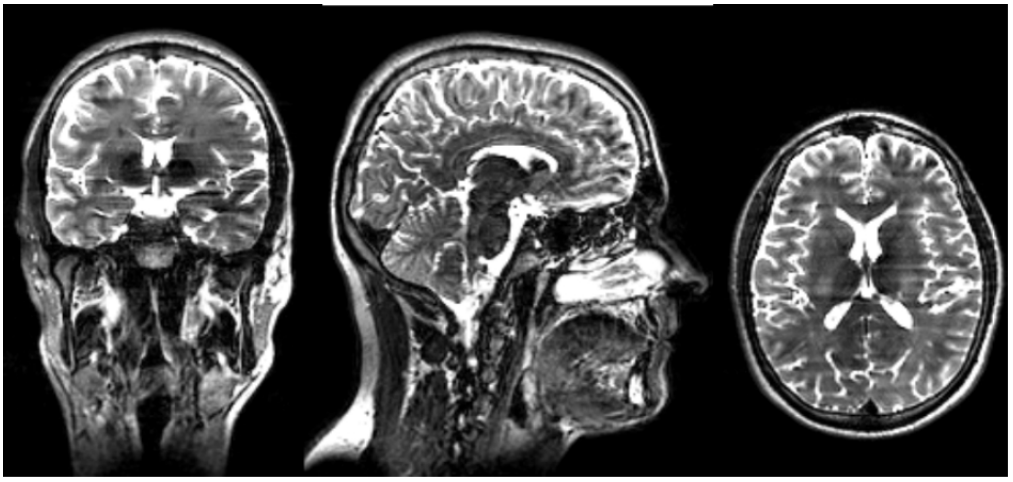

Figure 6.2: T2-weighted human MRI
Sagittal (left), coronal (middle) and axial (right) slice of a T2-image.

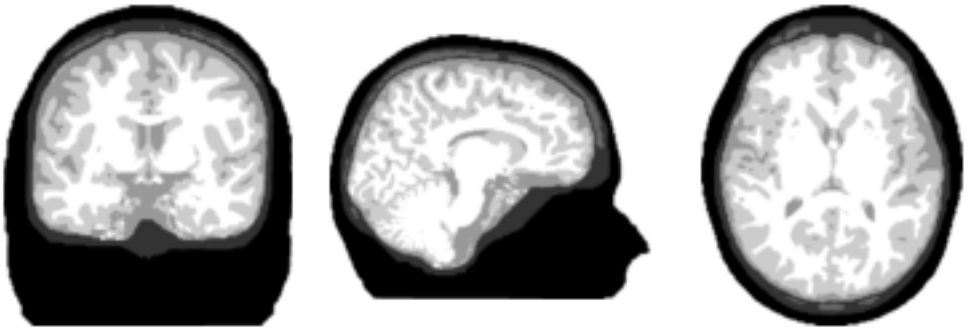

Figure 6.3: Segmentation of human head
Sagittal (left), coronal (middle) and axial (right) slice of the segmentation of the human head model.

the T1w- and T2w-MRI we are able to manually or automatically (i.e. segmentation software like FSL, Seg3D, SPM, etc.) obtain a segmentation of the different tissues.

Based on the segmentation we are able to generate a geometry-adapted hexahedral FE mesh (i.e. meshing toolboxex like vgrid). Additionally, we use the DW-MRI to calculate the conductivity tensors of the white matter. With these tensors we simulate the anisotropic conductivity the fiber tracts causes in white matter cause.

Another important aspect of the head model is the conductivities for the different tissues. These values are based on following papers: skin [23], skull compacta and spongiosa [10], CSF [24] and grey matter [25], and are shown in table 6.1.

Tissue	Conductivity(Sm $^{-1}$)
Skin	0.43
Skull compacta	0.007
Skull spongiosa	0.025
Electrodes	1.4
CSF	1.79
Brain gray matter	0.33
Brain white matter	anisotropic

Table 6.1: Conductivities of the different tissues.

6.2 Optimization with different approaches

In this section we will use different optimization approaches on predefined targets. We introduce the different targets and the electrode mask. After this we will formulate the optimization problems.

6.2.1 Targets and electrode mask

A brief overview about the targets and the electrode mask we want to use for stimulation is given in this section.
We have chosen four targets. A tangential, Fig. 6.9, a radial, Fig. 6.5, a deep tangential, Fig. 6.15 and a patch, Fig. 6.13 target. All of them are cortical and surface near targets on the frontal lobe, except the deep tangential which is is located deeper in the cortex as the other three.

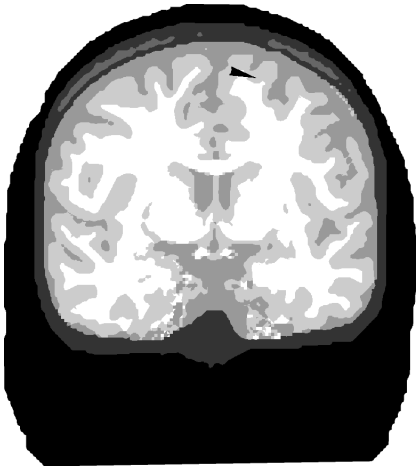

Figure 6.4: Tangential target vector

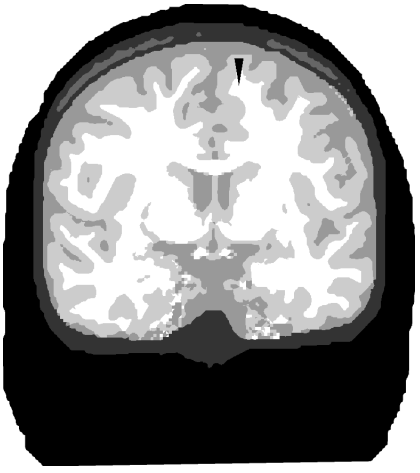

Figure 6.5: Radial target vector

For our electrode mask we use a extended 10-10 EEG electrode configuration with 74 electrodes (see figure 6.8). With this electrode configuration we should have a sufficient

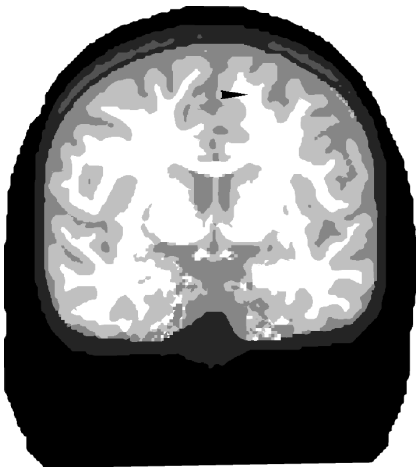

Figure 6.6: Deep tangential target vector

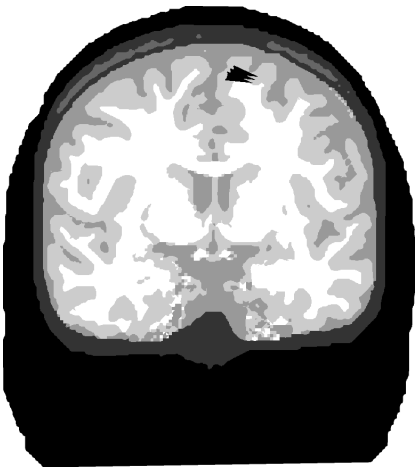

Figure 6.7: Patch target vector

coverage of the whole head. Important to mention is that these electrode position are fixed. The optimization approach just optimizes the stimulation protocol, not the position of the electrodes.

6.2.2 Approaches

We will now formulate the different optimization approaches. For the safety of the patient, all approaches need to fulfil a safety constrained. Thus we limit the total and individual current to 2mA (=: s_{max}) as in [1] suggested. As the sum of all positive electrodes is equal to the sum of all electrodes, we can also limit the sum of all absolute values by 4mA. In addition, we want to mention that the value of the reference electrode is the negative sum of all other electrodes, as we want to avoid (de)loading of the patient's head. Thus we can rewrite the constrained as:

$$2 \cdot s_{max} \geq \sum_{m=1}^{M} |s_m| = \sum_{m=2}^{M} |s_m| + |\sum_{m=2}^{M} s_m|.$$

Weighted least square

$$\begin{aligned} &\text{minimize } \|W(As - e)\|_2^2 \\ &\text{subject to } \sum |s_m| + |\sum s_m| \leq 2 \cdot s_{max} \end{aligned} \tag{6.1}$$

where $s \in \mathbb{R}^m$ $A \in \mathbb{R}^{n \times m}$, $W \in \mathbb{R}^{n \times n}$ $e \in \mathbb{R}^n$

The most interesting part of this approach is the weighting matrix W. W is a diagonal matrix and is defined as

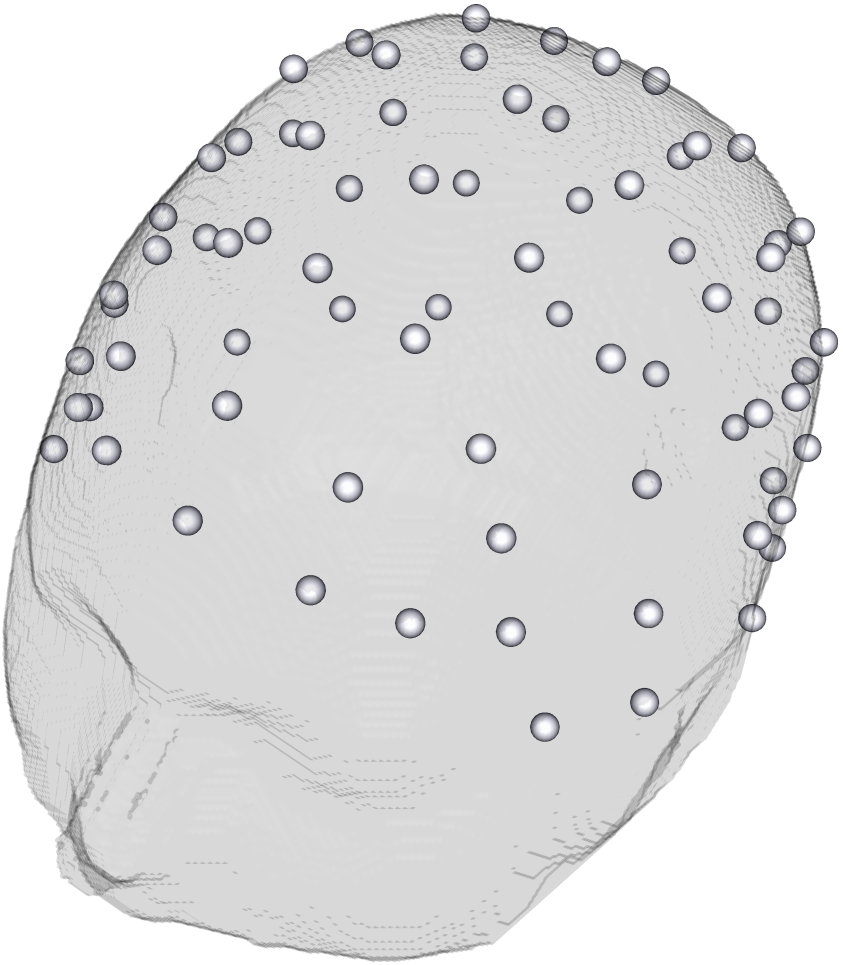

Figure 6.8: 10-10 system Electrode setup

$$W_{ij} = \begin{cases} \omega & \text{in } \mathbb{T} \wedge i = j \\ \omega^c & \text{in } \mathbb{T}^c \wedge i = j \\ 0 & i \neq j \end{cases} \tag{6.2}$$

where $\mathbb{T}$ is the predefined target region and ω, ω^c are the different weightings which fulfil $\frac{\omega|\mathbb{T}|}{\omega^c|\mathbb{T}^c|} = k$. So the the solution highly depends on k, which acts as a trade-off parameter for focality and intensity. In our approach we used $k = 1$ to counterbalance the difference of nodes in $\mathbb{T}$ and $\mathbb{T}^c$.

To solve this problem we use the method called least-absolute shrinkage and selection operator (lasso) [26]. Part of the inequality constrained is a ℓ^1- norm, $\sum |s_m| = \|s\|_1$. Therefore the lasso algorithm provides a sparse solution.

Linearly constrained minimum variance

$$\begin{aligned} &\text{minimize } \|As\|_2^2 \\ &\text{subject to } Cs = e \\ &\qquad \sum |s_m| + |\sum s_m| \leq 2 \cdot s_{max} \end{aligned} \tag{6.3}$$

where $x \in \mathbb{R}^m$ $A \in \mathbb{R}^{n \times m}$, $C = [a_{i1} a_{i2} \cdots a_{im}]$, $e \in \mathbb{R}^3$

The most interesting part of this approach is the definition of C. If we multiply C with an artificial stimulation protocol s, we receive the electric field at the target node. Thus we can specify the desired direction and intensity at the target with e.

To solve this problem we used the toolbox CVX mentioned in [27]. This toolbox provides tools for disciplined convex programming and therefore a solver for 6.3.

Maximal intensity

$$\begin{aligned} &\text{maximize } f(x) = e^T C x \\ &\text{subject to } \sum |s_m| + |\sum s_m| \leq 2 \cdot s_{max} \end{aligned} \tag{6.4}$$

This approach is straight forward. We specify a desired target with C and a desired direction with e^T. The only limitations set is the applied current, there is no penalization of wide spread stimulation, thus leading to a very broad but intense stimulus.

Alternating direction method of multipliers

$$\begin{aligned} \text{minimize } f(s) \quad &= -\int_{\Omega_t} \langle As, e \rangle + \alpha \int_{\Gamma} s^2 dx + \beta ||s||_{\mathbb{M}(\Gamma)} \\ \text{subject to } \omega |As| \quad &\leq \epsilon \end{aligned} \tag{6.5}$$

This formulation of the optimization problem and the algorithm for a solution was developed in [2], which is highly recommended for further reading. The first term of the minimization problem favours solution with the right direction and high intensity at the target. It has the highest value if the direction at the target node is the same as the desired target, 0 if it is orthogonal, and, in a worst case, it has the opposite direction. The second term penalizes concentrated applied current, thus leading to a spread stimulation protocol in terms of applied current. The last term provides sparseness for the solution. In addition, the constraint provides focality as it forces the overall field outside the target region to be below a certain value ϵ.

6.3 Characteristic numbers

In this section we introduce some unitless charistic numbers that help us to understand and compare the outcomes of the different approaches.

Average intensity at the target region

One of the most interesting part of stimulation is what applied current we can reach at our target region as it is the main part we focus on in brain stimulation. This will be computed as

$$\mathrm{IT} = \frac{\int_{\Omega_t} |\boldsymbol{A}\boldsymbol{s}| \, \mathrm{d}\boldsymbol{x}}{|\Omega_t|}. \tag{6.6}$$

Average Intensity at the non target region

In contrast to IT we will also compute the average intensity at the non target region as

$$\mathrm{INT} = \frac{\int_{\Omega \setminus \Omega_t} |\boldsymbol{A}\boldsymbol{s}| \, \mathrm{d}\boldsymbol{x}}{|\Omega \setminus \Omega_t|} \tag{6.7}$$

to get a better understanding of the focality.

Direction of the current flow in the target region

Another interesting aspect to consider is the scalar product of the applied current and the desired current in the target region. It is computed as

$$\mathrm{DIR} = \frac{\int_{\Omega} \langle \boldsymbol{A}\boldsymbol{s}, \boldsymbol{e} \rangle \, \mathrm{d}\boldsymbol{x}}{|\Omega_t|} \tag{6.8}$$

Focality

In brain stimulation it is often the case that one want to stimulate a specific region of the brain. However to reach certain targets we also have to stimulate other regions. The following measure provides some insight of the actual focality of the applied current.

$$\mathrm{FOC} = \frac{IT}{INT} \tag{6.9}$$

Corrected earth mover's distance

In addition to FOC we will introduce another measure to compare the focality of the applied current. For this we make use of the earth mover's distance (see 3.7).

$$cEMD = \frac{EMD(As, e)}{IT} \tag{6.10}$$

We normalize the EMD by IT to make this measure more comparable. I.e. if we double the applied current at every electrode, the current density field would be doubled and therefore we would obtain a doubled EMD.

Parallelity

Another important factor to look at is the amount of current density that flows parallel to our target. It is evaluated as

$$PAR = \frac{DIR}{IT} \tag{6.11}$$

6.4 Comparison of the different optimization approaches

We show the stimulation protocols and applied current density for the different targets and give the characteristic numbers to compare the different approaches.

6.4.1 Tangential target

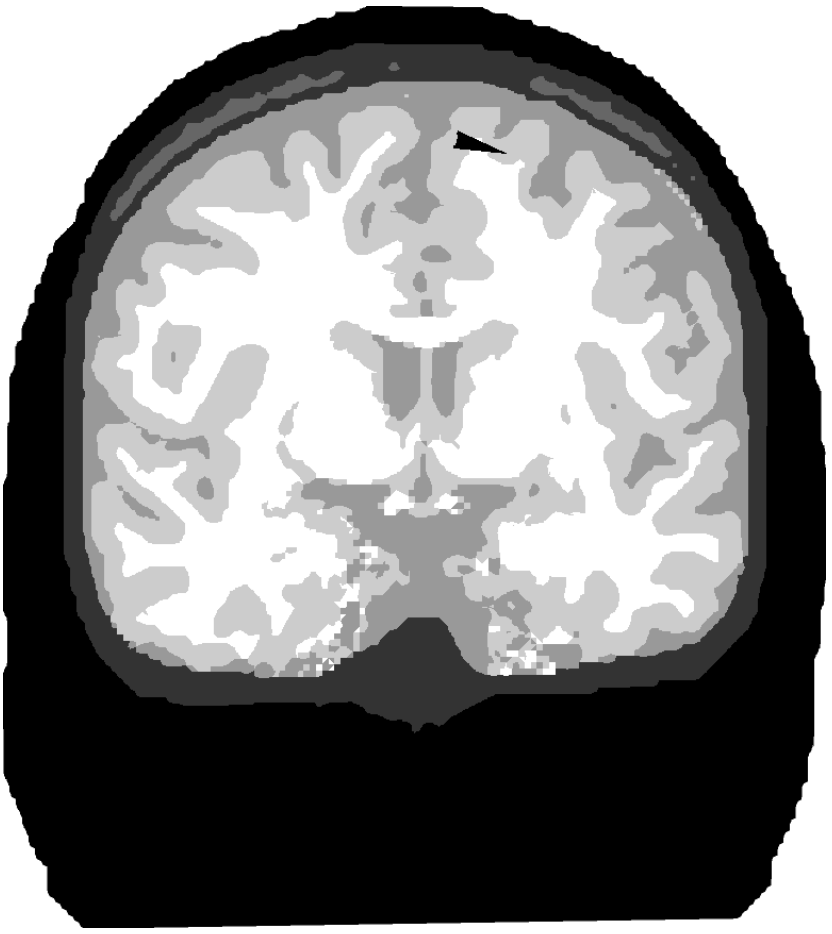

Figure 6.9: Tangential target vector

		$[Am^{-2}]$				[%]
Method	IT	INT	DIR	FOC	cEMD	PAR
LCMV	0.03196	0.00145	0.03079	22.04	1263	**96.34%**
ADMM	0.03785	0.00151	0.03302	**25.07**	**1096**	87.24%
W-LS	0.09077	0.00527	0.08262	17.22	1647	91.02%
max. Intensity	**0.21188**	0.04657	0.19783	4.55	7911	93.37%

Table 6.2: Characteristic values for the simulation of tangential target stimulation.

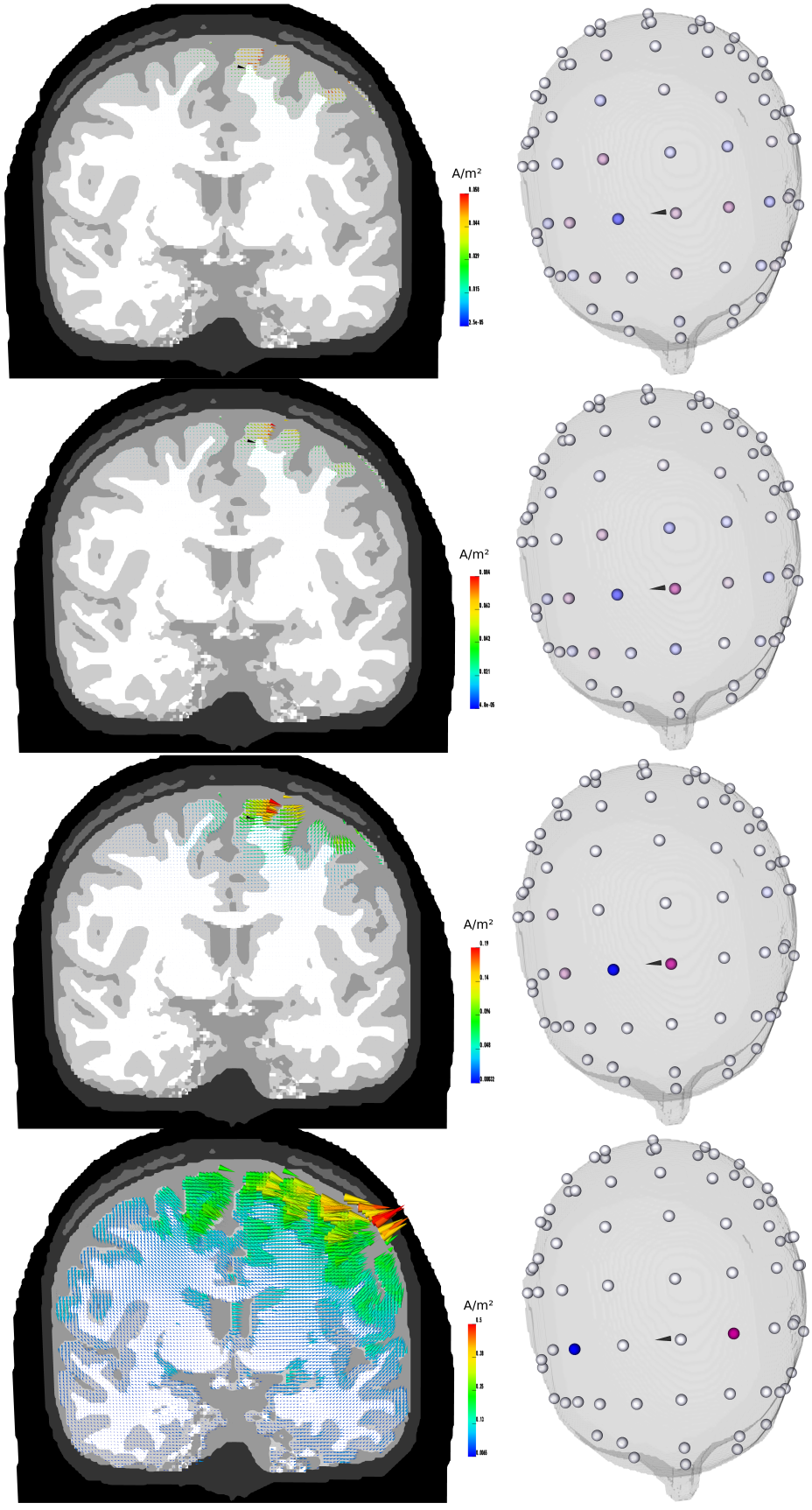

Figure 6.10: Stimulation protocols for the tangential target (from top to bottom: LCMV, ADMM, W-LS, max. Intensity.)

Radial target

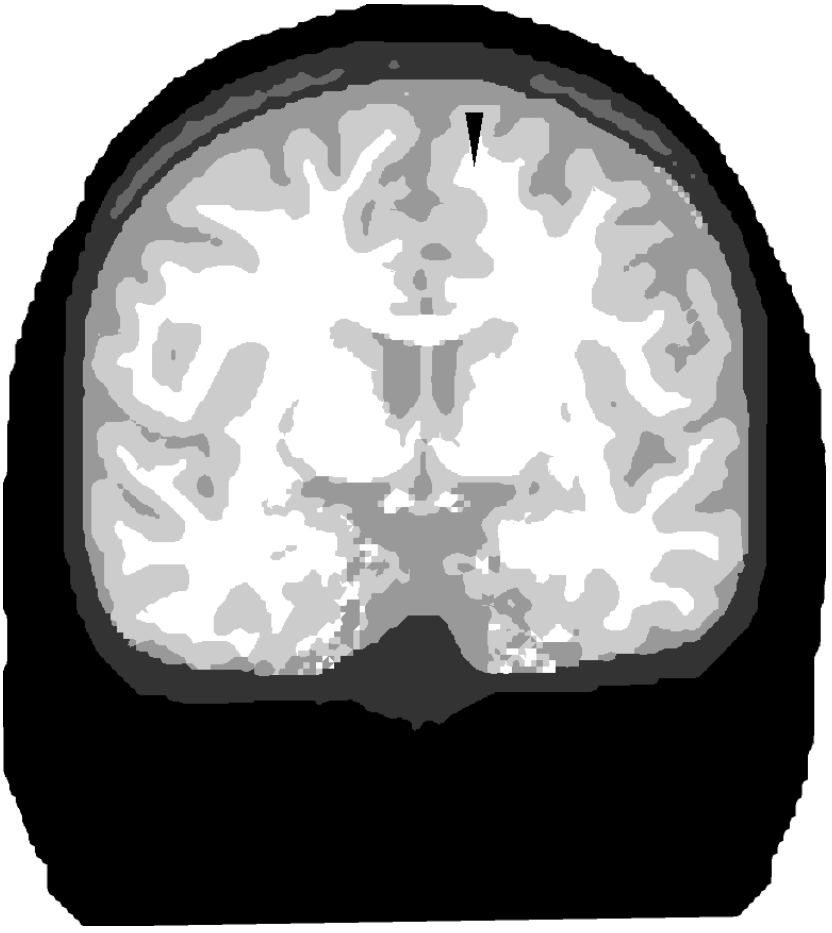

Figure 6.11: Radial target vector

		$[Am^{-2}]$				[%]
Method	IT	INT	DIR	FOC	cEMD	PAR
LCMV	0.03325	0.000695	0.03325	47.84	995	**100%**
ADMM	0.04504	0.00071	0.04341	**63.44**	**671**	96.38%
W-LS	0.07190	0.00154	0.06952	46.69	975	96.69%
max. Intensity	**0.19844**	0.04890	0.18307	4.06	19729	92.25%

Table 6.3: Characteristic values for the simulation of a radial target stimulation.

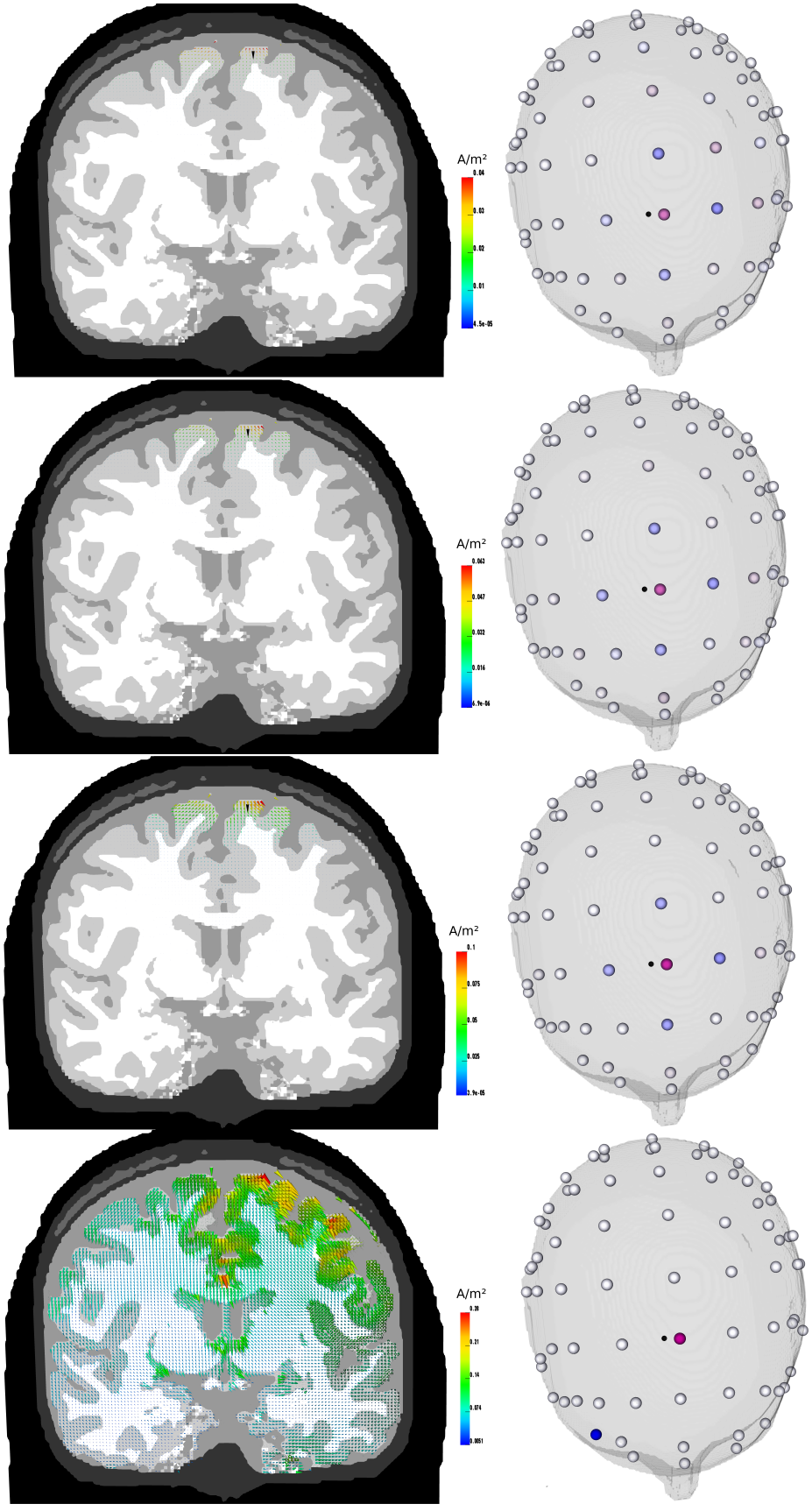

Figure 6.12: Stimulation protocols for the radial target (from top to bottom: LCMV, ADMM, W-LS, max. Intensity.)

Patch target

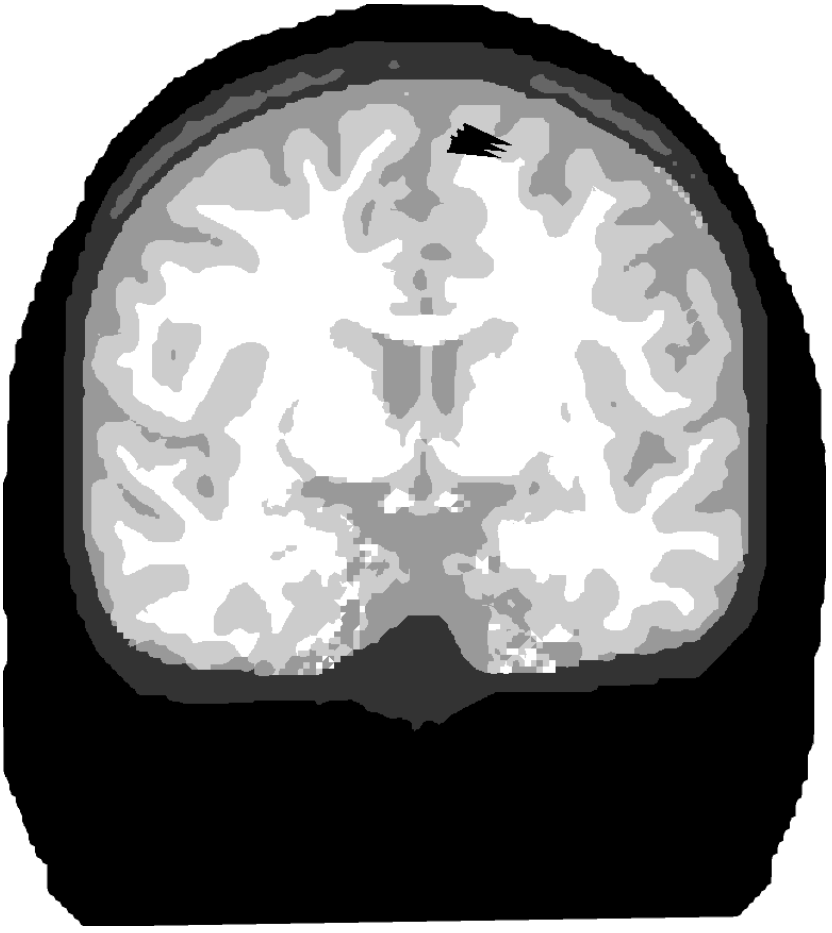

Figure 6.13: Patch target vector

		$[Am^{-2}]$				[%]
Method	IT	INT	DIR	FOC	cEMD	PAR
LCMV	0.11490	0.00978	0.10708	11.75	3278	93.19%
ADMM	0.03700	0.00157	0.03330	**23.57**	**1123**	90.00%
W-LS	0.07329	0.00356	0.06667	20.59	1250	90.97%
max. Intensity	**0.21195**	0.04657	0.19883	4.55	7872	**93.80%**

Table 6.4: Characteristic values for the simulation of a patch target stimulation.

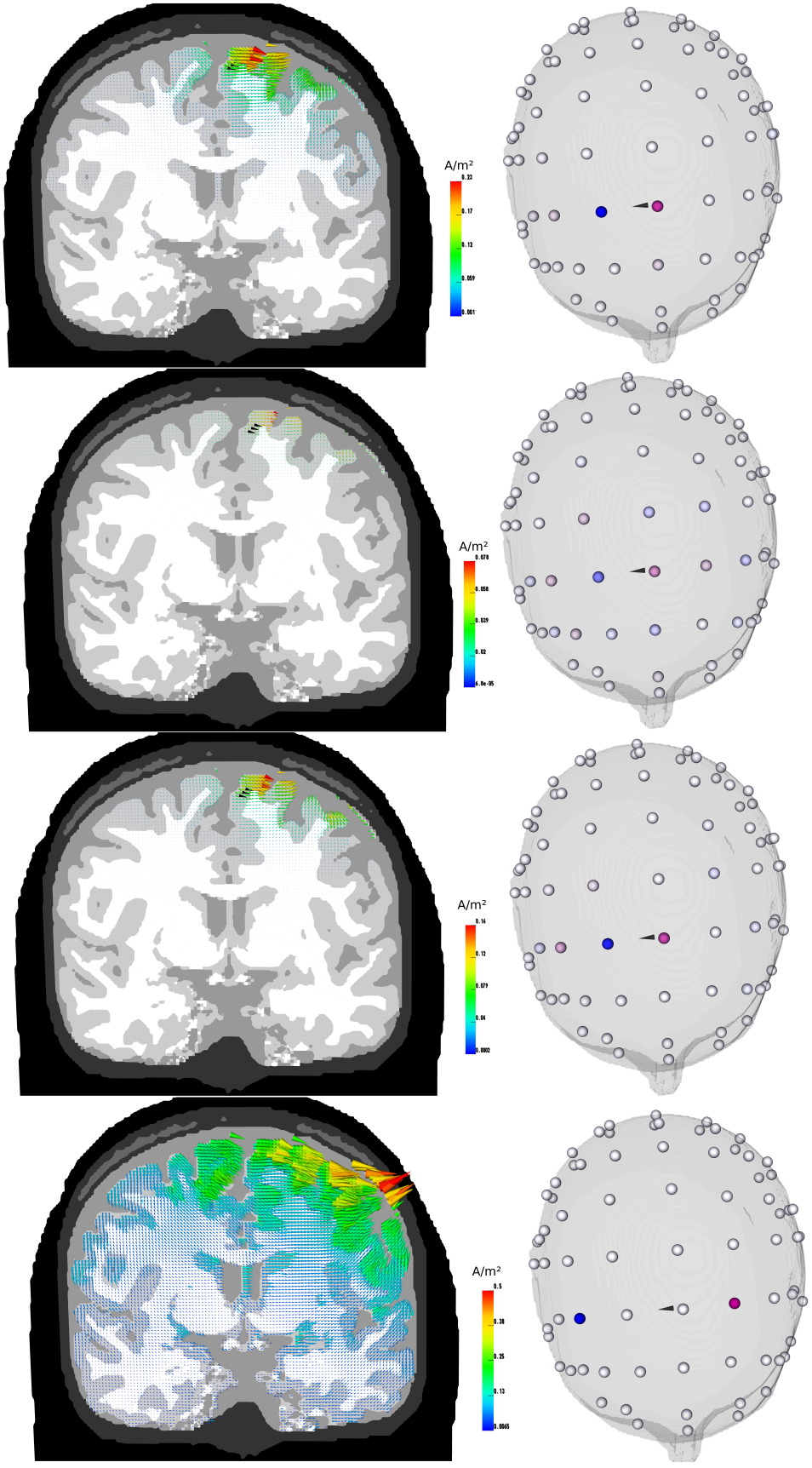

Figure 6.14: Stimulation protocols for the patch target (from top to bottom: LCMV, ADMM, W-LS, max. Intensity.)

Deep tangential target

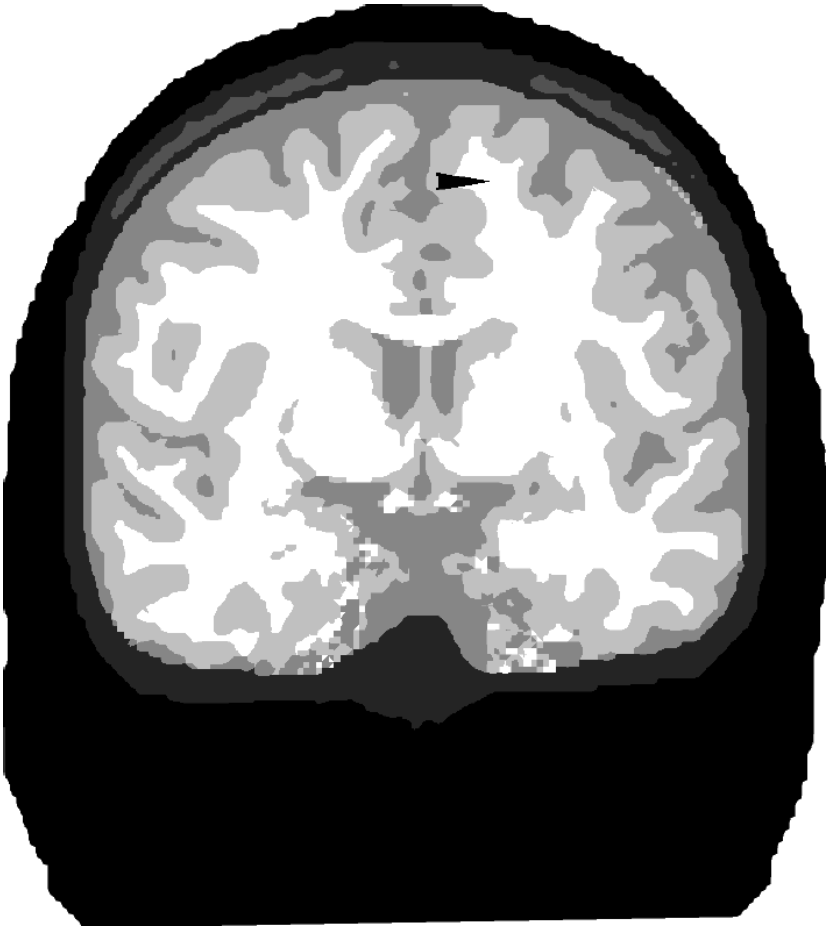

Figure 6.15: Deep tangential target vector

		$[Am^{-2}]$				[%]
Method	IT	INT	DIR	FOC	cEMD	PAR
LCMV	0.03180	0.00494	0.03162	6.44	4759	**99.43%**
ADMM	0.01883	0.00249	0.01765	**7.56**	**2153**	96.29%
W-LS	0.08231	0.01973	0.08061	4.17	9144	97.93%
max. Intensity	**0.11700**	0.05662	0.11476	2.07	21511	98.09%

Table 6.5: Characteristic values for the simulation of deep tangential target stimulation.

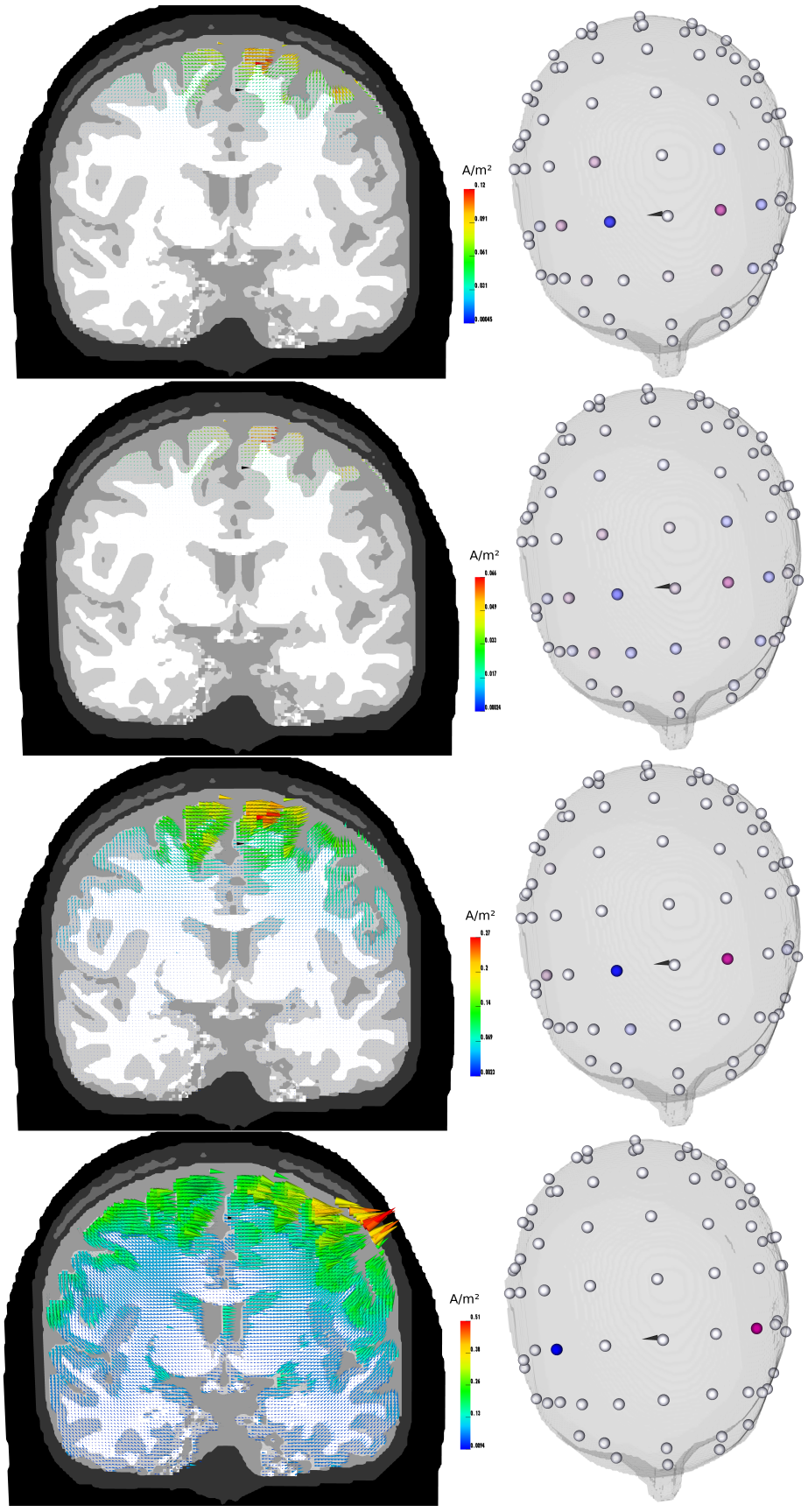

Figure 6.16: Stimulation protocols for the deep tangential target (from top to bottom: LCMV, ADMM, W-LS, max. Intensity.)

Summary

			$[Am^{-2}]$				[%]
Target	**Method**	IT	INT	DIR	FOC	cEMD	PAR
tangential	LCMV	0.03196	0.00145	0.03079	22.04	1263	**96.34%**
	ADMM	0.03785	0.00151	0.03302	**25.07**	**1096**	87.24%
	W-LS	0.09077	0.00527	0.08262	17.22	1647	91.02%
	max. Intensity	**0.21188**	0.04657	0.19783	4.55	7911	93.37%
radial	LCMV	0.03325	0.000695	0.03325	47.84	995	**100%**
	ADMM	0.04504	0.00071	0.04341	**63.44**	**671**	96.38%
	W-LS	0.07190	0.00154	0.06952	46.69	975	96.69%
	max. Intensity	**0.19844**	0.04890	0.18307	4.06	19729	92.25%
patch	LCMV	0.11490	0.00978	0.10708	11.75	3278	93.19%
	ADMM	0.03700	0.00157	0.03330	**23.57**	**1123**	90.00%
	W-LS	0.07329	0.00356	0.06667	20.59	1250	90.97%
	max. Intensity	**0.21195**	0.04657	0.19883	4.55	7872	**93.80%**
deep tang.	LCMV	0.03180	0.00494	0.03162	6.44	4759	**99.43%**
	ADMM	0.01883	0.00249	0.01765	**7.56**	**2153**	96.29%
	W-LS	0.08231	0.01973	0.08061	4.17	9144	97.93%
	max. Intensity	**0.11700**	0.05662	0.11476	2.07	21511	98.09%

Table 6.6: Characteristic values for all simulations.

In terms of IT we see that max. Intensity performs best in any given target. This seems reasonable as it is not restricted to any focality optimization. If we look close to the formulation (6.4) we only see an interest in maximizing the intensity.

If we look at the FOC and cEMD ADMM performs best in all cases. A close look at the formulation (6.5) shows that the constraint favours low currents in the non-target region.

LCMV provides good results in terms of PAR. Despite the patch target it performs best in all other cases. This also seems reasonable as the LCMV formulation (6.3) favours solution with a small difference between desired and actual solution.

This simulation shows that the experimenter has to be aware of what stimulation is optimal, as the before discussed methods can only provide guidance when the needs and demands of the experiment are defined.

6.5 Two-target stimulation

In some cases it is interesting to stimulate two regions at the same time. In this section we will compare the different approaches from the previous section on how they perform on stimulation of two-targets. For this we use the same electrode setup as in 6.2.1.

6.5.1 Targets

The targets we used are two artificial tangential targets.

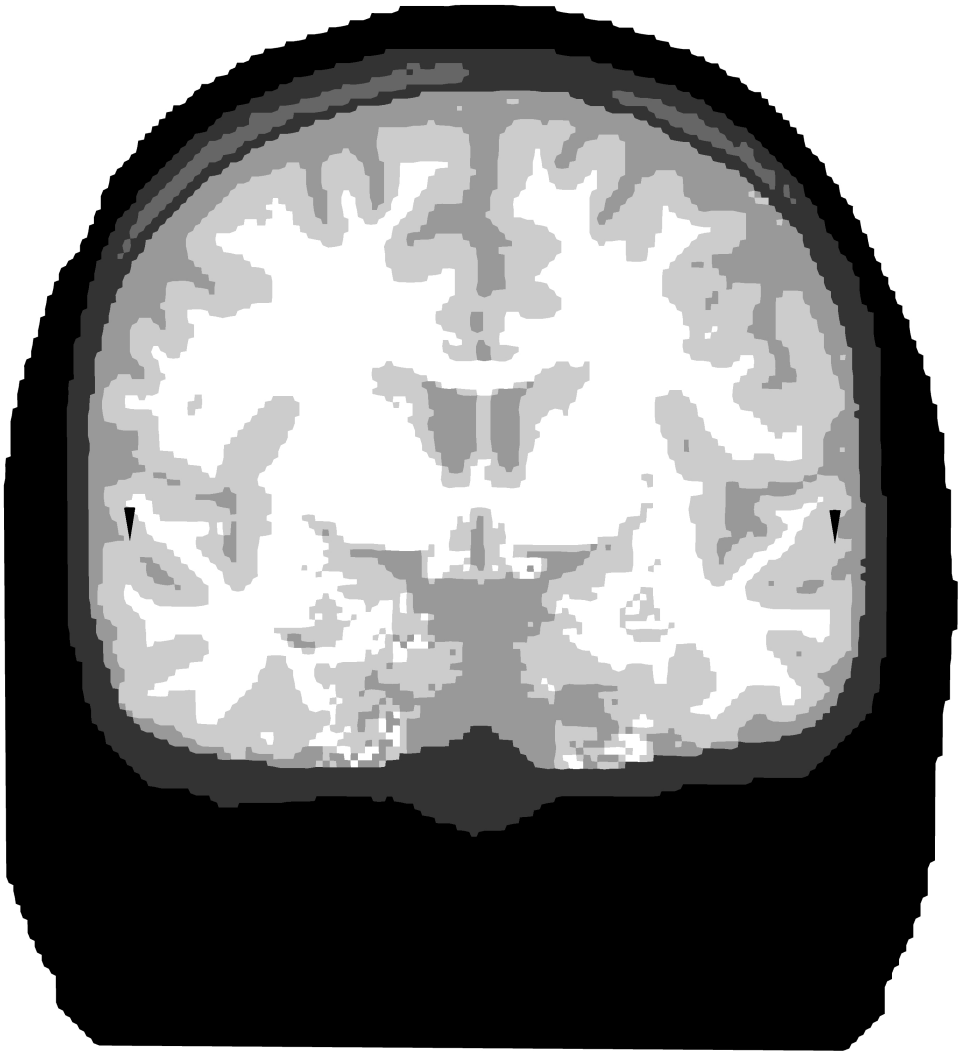

Figure 6.17: Two tangential targets

6.5.2 Evaluation

We will look at the different current density maps and stimulation protocols to evaluate the different approaches. What we are interested in is how the approaches behave on a

two-target setup or if they are even applicable for this problem.

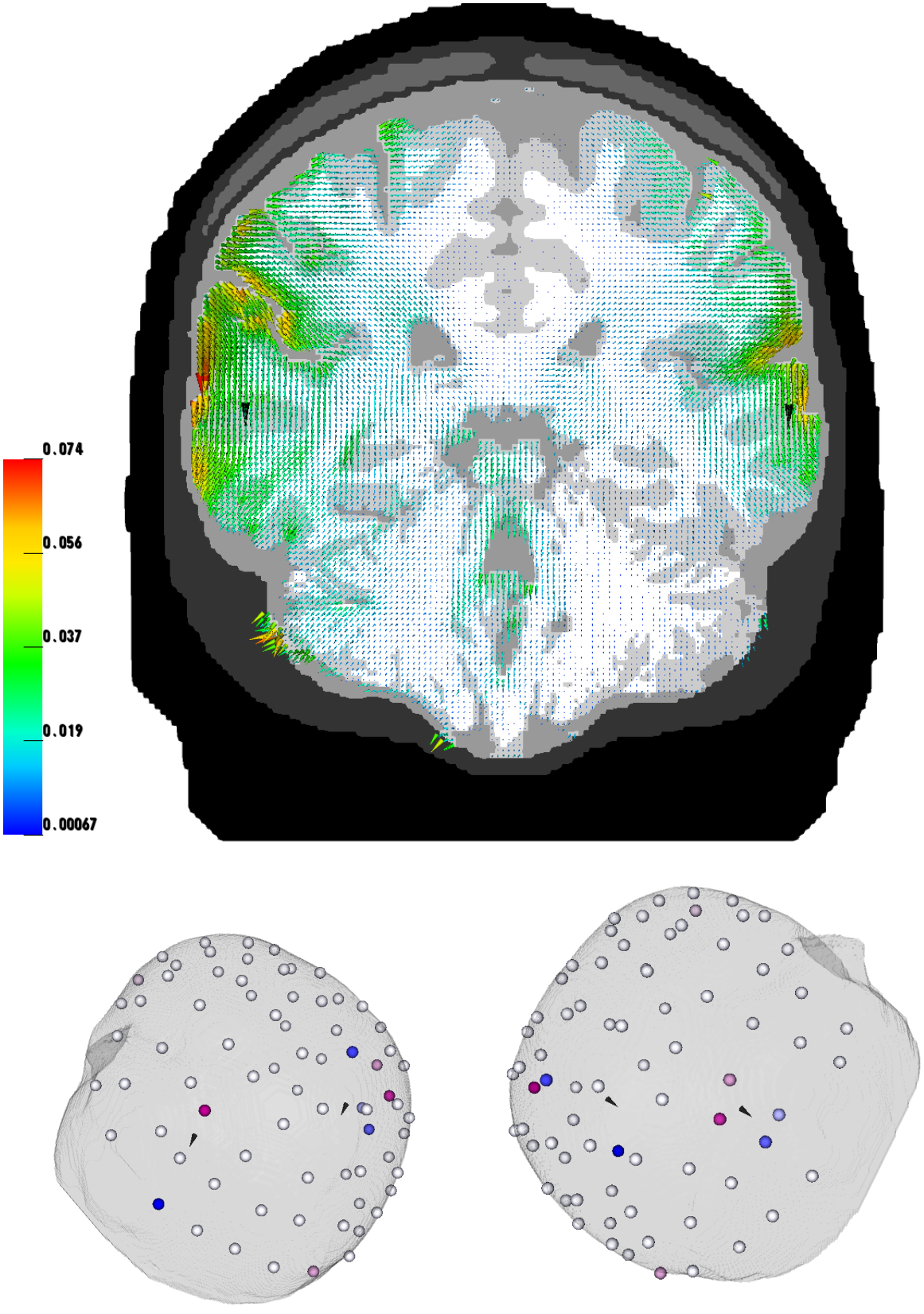

Figure 6.18: LCMV optimization for two-target setup

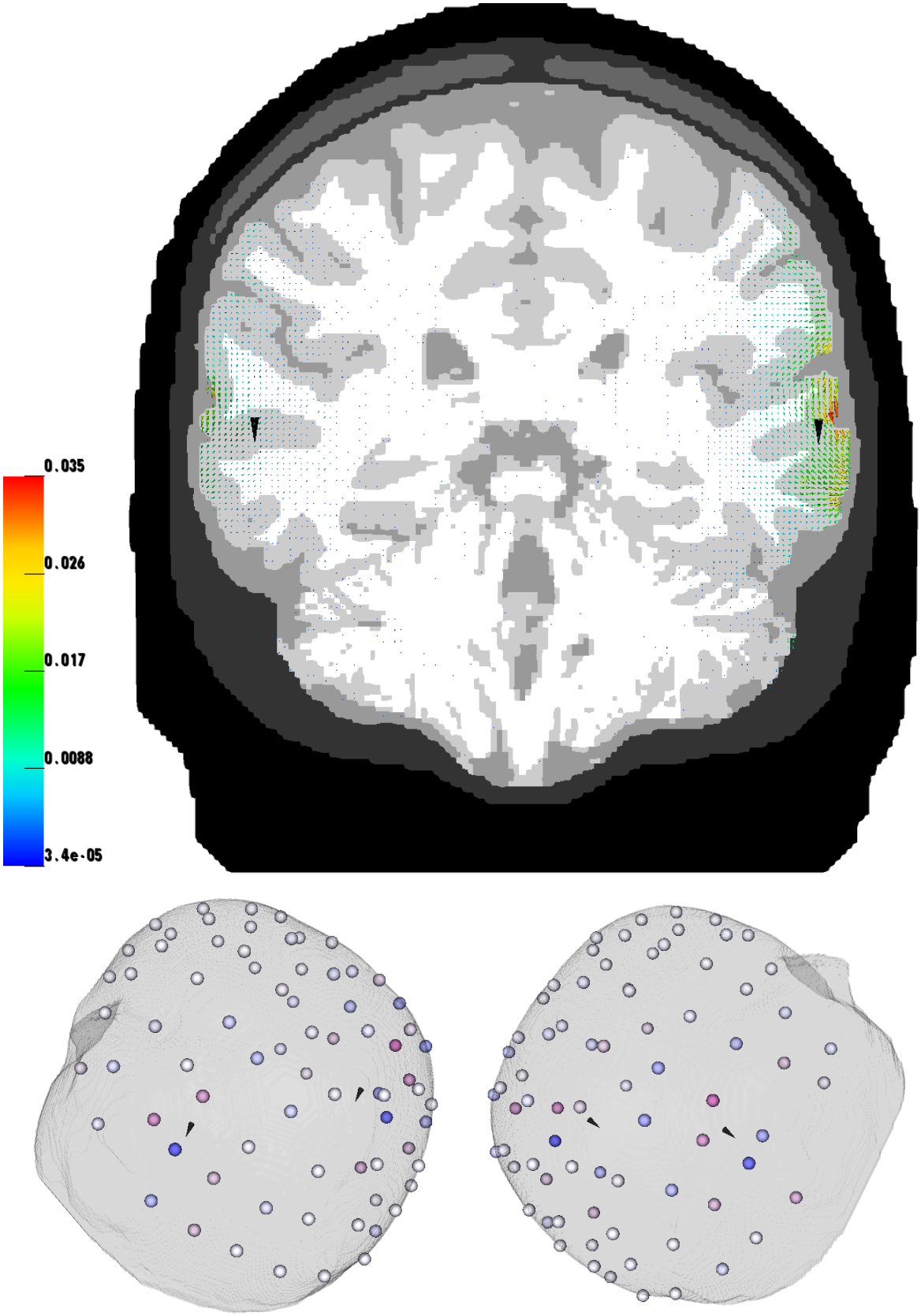

Figure 6.19: ADDM optimization for two-target setup

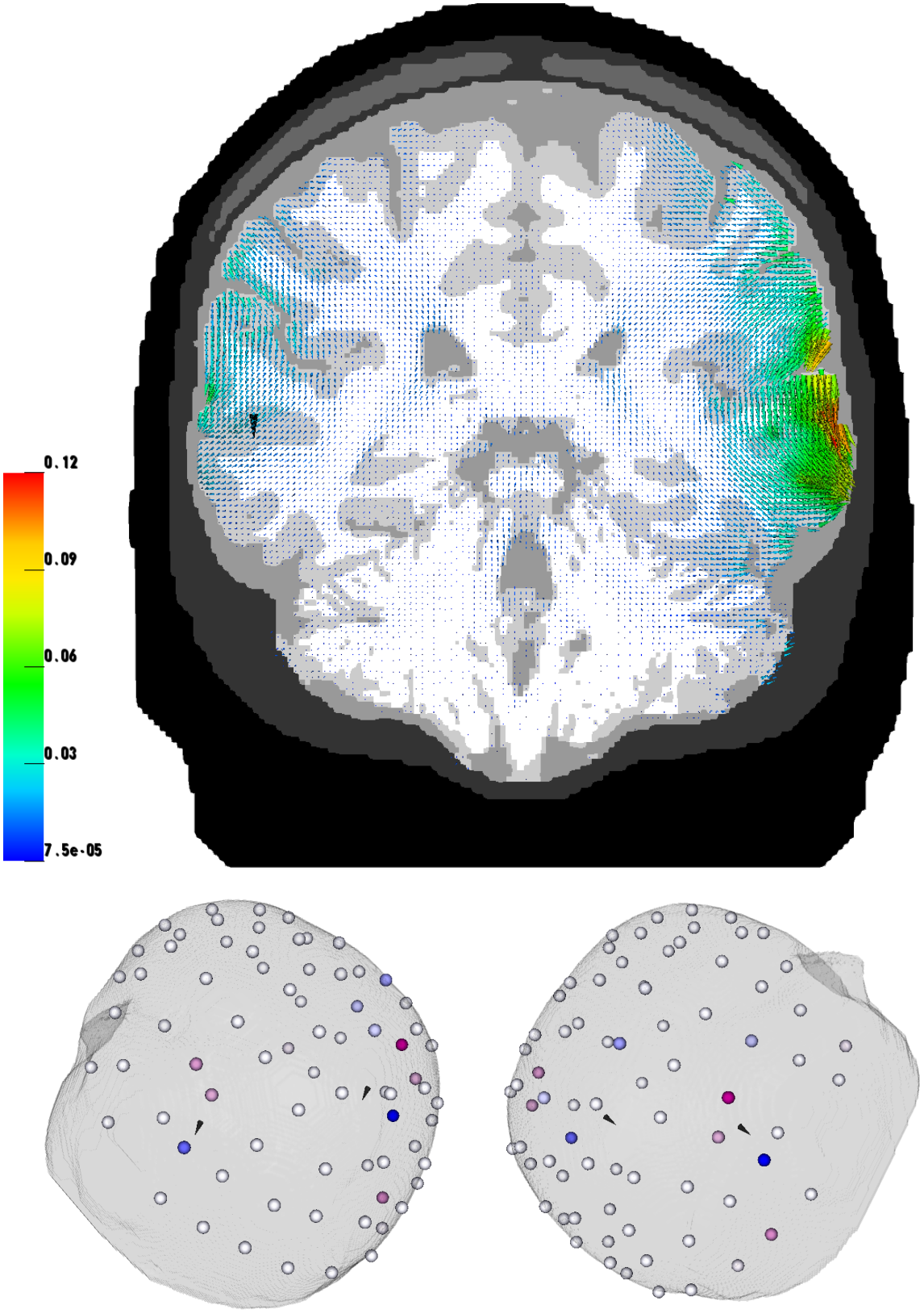

Figure 6.20: W-LS optimization for two-target setup

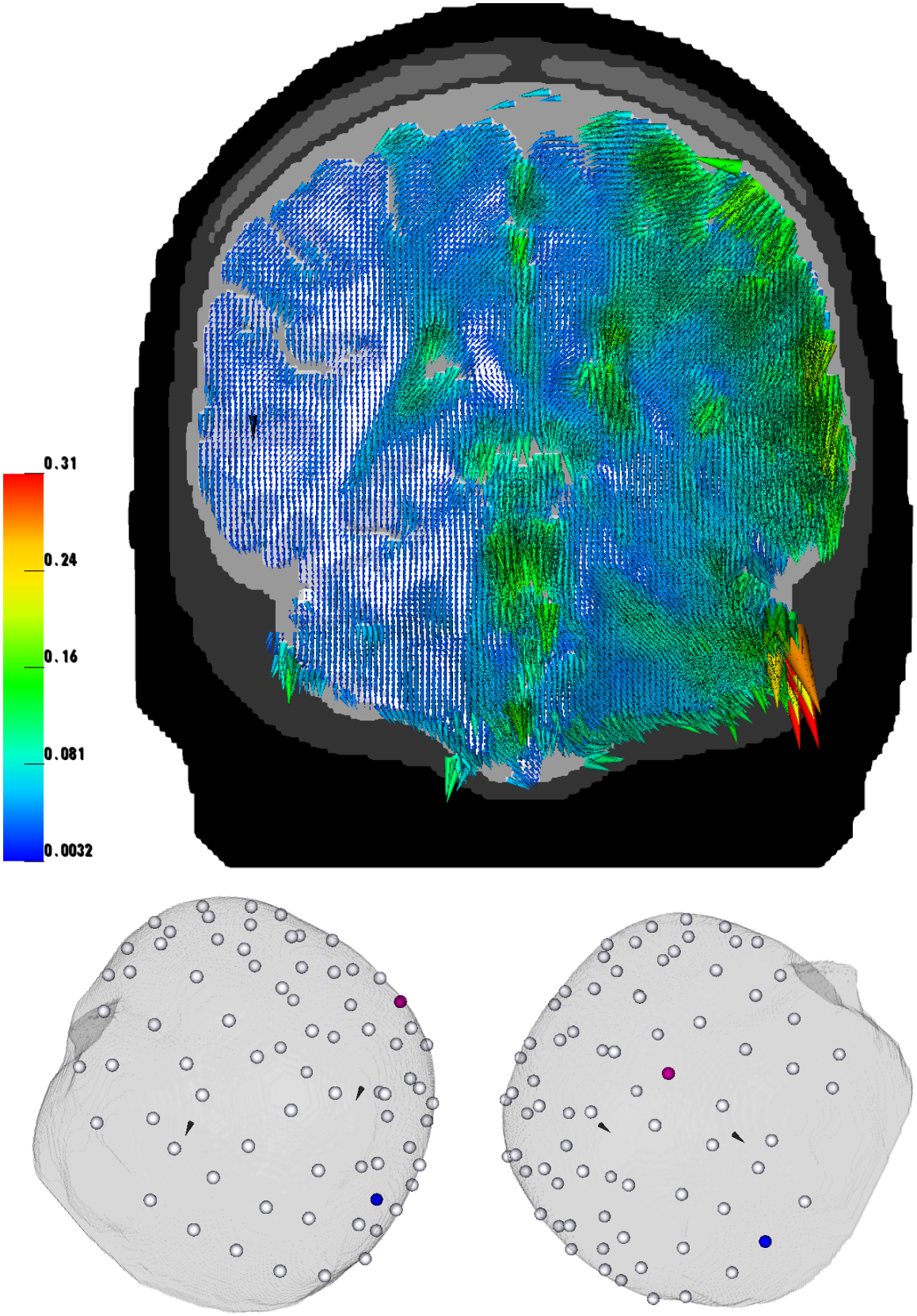

Figure 6.21: Max. Intensity optimization for two-target setup

			$[Am^{-2}]$			[%]	
Method	IT-L	IT-R	INT	DIR-l	DIR-r	PAR-l	PAR-r
LCMV	0.03234	0.03184	0.01450	0.03234	0.03184	**100**%	**100**%
ADMM	0.01048	0.02101	**0.00183**	0.00754	0.01546	71.94%	73.58%
W-LS	0.02388	0.07358	0.00947	0.01815	0.05297	76.00%	71.98%
max. Intensity	**0.03327**	0.**12595**	0.06340	0.03031	0.10772	91.10%	85.52 %

First we have a look at the different IT values. In all approaches we see an imbalance in the achieved IT. The target on the right side seem to got higher IT values than the left ones. The only exception is the LCMV approach which yields nearly the same IT for both targets.

In additon we see a good performance with regards to PAR in LCMV. Both targets are stimulated perfectly in the right direction. The other approaches only carry out PAR values far below LCMV.

As a conclusion of this simulation we suggest the LCMV approach for a two-target stimulation.

6.6 Misspecification of target angle

In this section we want to analyse the influence of a misspecification of the angle of a target. As shown in [28], and [15] the direction of stimulation is very important. However in practice the specification might not be very accurate. Therefore, the computed stimulation protocol doesn't fit perfectly for the desired target.

6.6.1 Targets

As target we choose a deep location with tangential orientation. Furthermore we define 4 distorted targets. All of them have angle difference of 8° from the right target. In all cases the location is still the same.

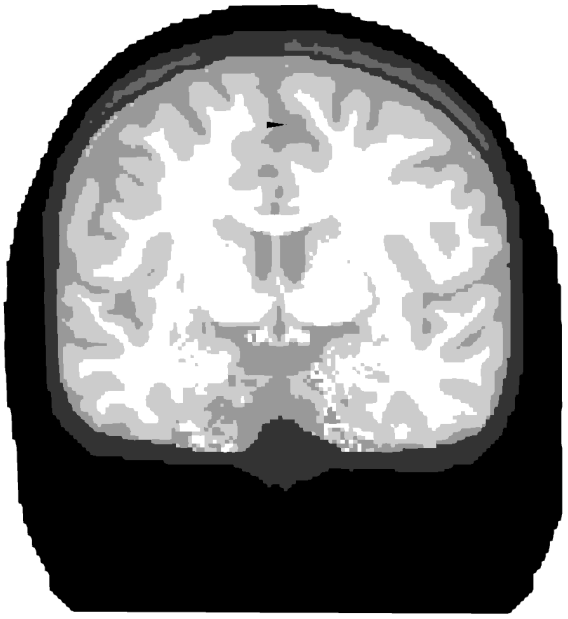

Figure 6.22: Deep tangential target with right angle

6.6.2 Evaluation

First of all we will define some new indicators for our evaluation.

Relative direction of the current flow in the target region

This measure is nearly the same as DIR with the small difference that we compute the scalar product from the original target despite the disorientated one.

$$rDIR = \frac{\int_\Omega \langle \boldsymbol{As}, \boldsymbol{e}_{original} \rangle \, \mathrm{d}\boldsymbol{x}}{|\Omega_t|} \tag{6.12}$$

Relative parallelity

Respectively to rDIR the relative parallelity considers the intensity of the original target.

$$rPAR = \frac{rDIR}{IT} \tag{6.13}$$

			$[Am^{-2}]$			[%]
Target	**Method**	IT	INT	rDIR	FOC	$rPAR$
original	LCMV	0.03356	0.00818	0.03356	4.10	**100%**
	ADMM	0.01860	**0.00165**	0.01752	**11.27**	94.19%
	W-LS	0.05552	0.01204	0.05136	4.61	92.50%
	max. Intensity	**0.10304**	0.04226	0.9658	2.43	93.73%
1st misangled	LCMV	0.2049	0.00653	0.01866	3.14	91.06%
	ADMM	0.01878	**0.00168**	0.01758	**11.17**	93.61%
	W-LS	0.06782	0.01567	0.05922	4.32	87.31%
	max. Intensity	**0.10304**	0.04225	0.09658	2.43	**93.73%**
2nd misangled	LCMV	0.02253	0.00698	0.02052	3.23	91.08%
	ADMM	0.01800	**0.00158**	0.01694	**11.39**	**94.11%**
	W-LS	0.04896	0.00999	0.04030	4.90	82.31%
	max. Intensity	**0.10304**	0.04225	0.09658	2.43	93.73%
3rd misangled	LCMV	0.02302	0.00725	0.02097	3.17	91.09%
	ADMM	0.01850	**0.00163**	0.01710	**11.34**	92.43%
	W-LS	0.05702	0.01238	0.05204	4.60	91.26%
	max. Intensity	**0.10304**	0.04225	0.09658	2.43	**93.73%**
4th misangled	LCMV	0.02152	0.00679	0.01960	3.17	91.08%
	ADMM	0.01858	**0.00167**	0.01782	**11.13**	**95.90%**
	W-LS	0.05366	0.01163	0.05036	4.62	93.85%
	max. Intensity	**0.10304**	0.04225	0.09658	2.43	93.73%

Table 6.7: Characteristic values of the original and the four distorted targets.

LCMV is very sensitive to misspecification of the angle. In any given case it loses 9% of its PAR and 33% of its IT.

ADMM performs very robust to this misspecification. Every characteristic number in any simulation is nearly the same.

W-LS is also very sensitive. In some cases the performance is increased and in other it is decreased, but no direct correlation can be concluded.

The max. Intensity approach is the most robust one, as it isn't affected at all by the misspecification.

7 Simulation: Ferret

Validation of tDCS simulation in humans is quite difficult. Using depth electrodes to measure the ongoing stimulation is invasive, and therefore not optimal.

However, performing the same technique in ferrets is another option to validate the tDCS simulations. Therefore, we provide a highly-realistic FE 4-compartment isotropic ferret head model which can be used for tDCS simulation.

Based on this model we optimize the stimulation protocol with different approaches and compare these with the characteristic values we developed in the previous chapter.

7.1 Ferret head model

First of all we set up the highly-realistic ferret head model. For this we have used a T2w-MRI to obtain a segmentation of the desired tissues.

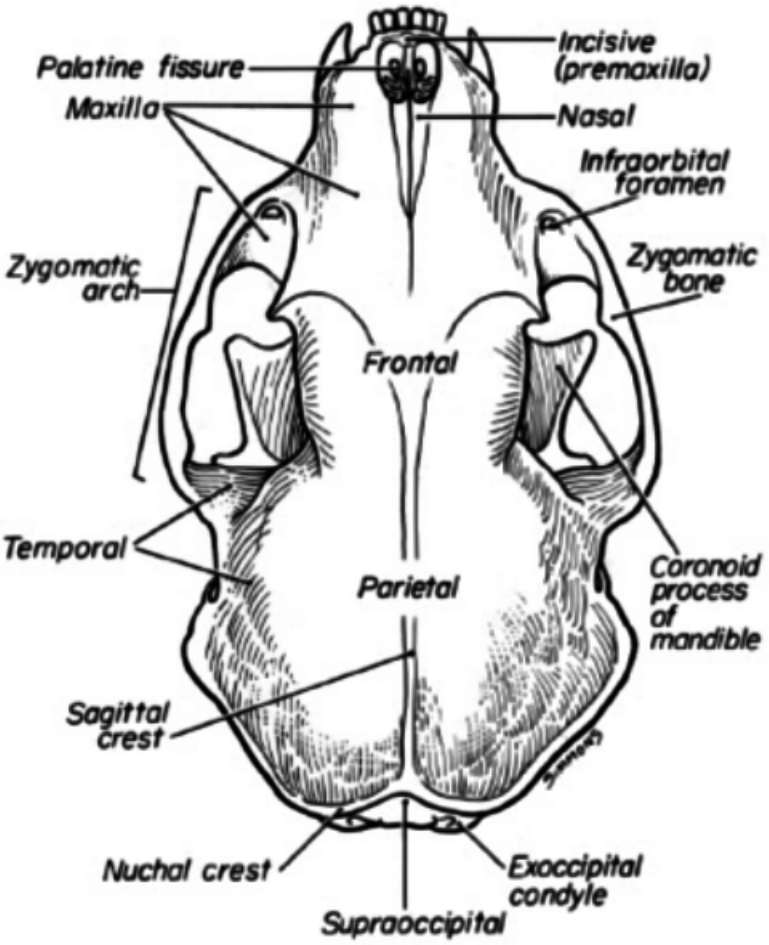

Figure 7.1: Atlas of a ferret skull
[29]

Figure 7.2: Slice of the MRI of a ferret
sagittal (left), coronal (middle) and axial (right)

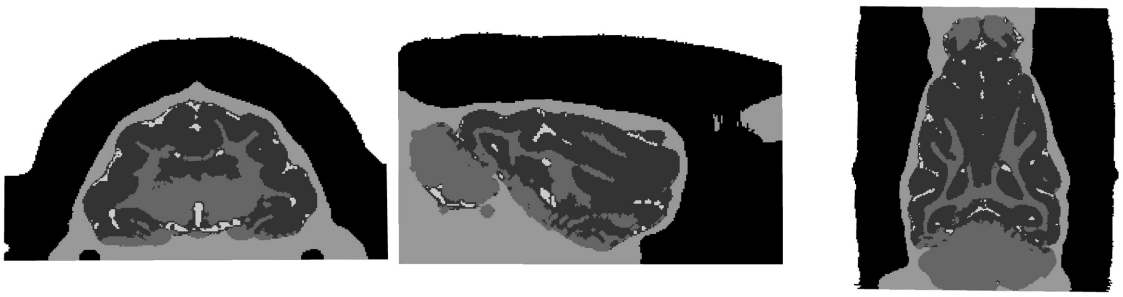

Figure 7.3: Slice of the segmentation of the ferret head model sagittal (left), coronal (middle) and axial (right)

Finding conductivity values for ferret tissues is quite difficult. Therefore we used tissue conductivity from other species to match them to the ferret. We used conductivity data from rats which was obtained in [30].

Tissue	Conductivity(Sm $^{-1}$)
Skin	0.33
Skull	0.042
CSF	1.79
White Matter	0.14
Grey Matter	0.33
Electrodes	1.4

Figure 7.4: Conductivities for ferret

7.2 Electrode setup and stimulation protocol

We want to perform a simulation of a simple stimulation. We use only four electrodes placed on the back of the head. The stimulation is a front-back and a right-left stimulation. As in practice we are able to stimulate on the skull we removed the skin in our model.

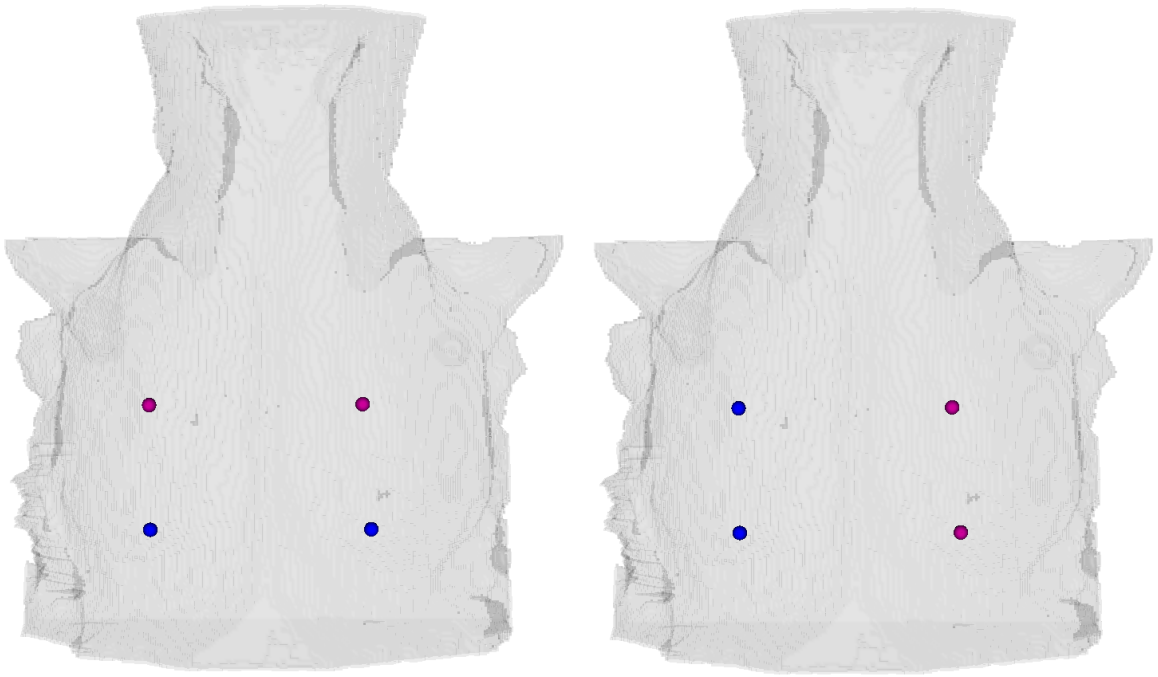

Figure 7.5: Simple stimulation protocoll

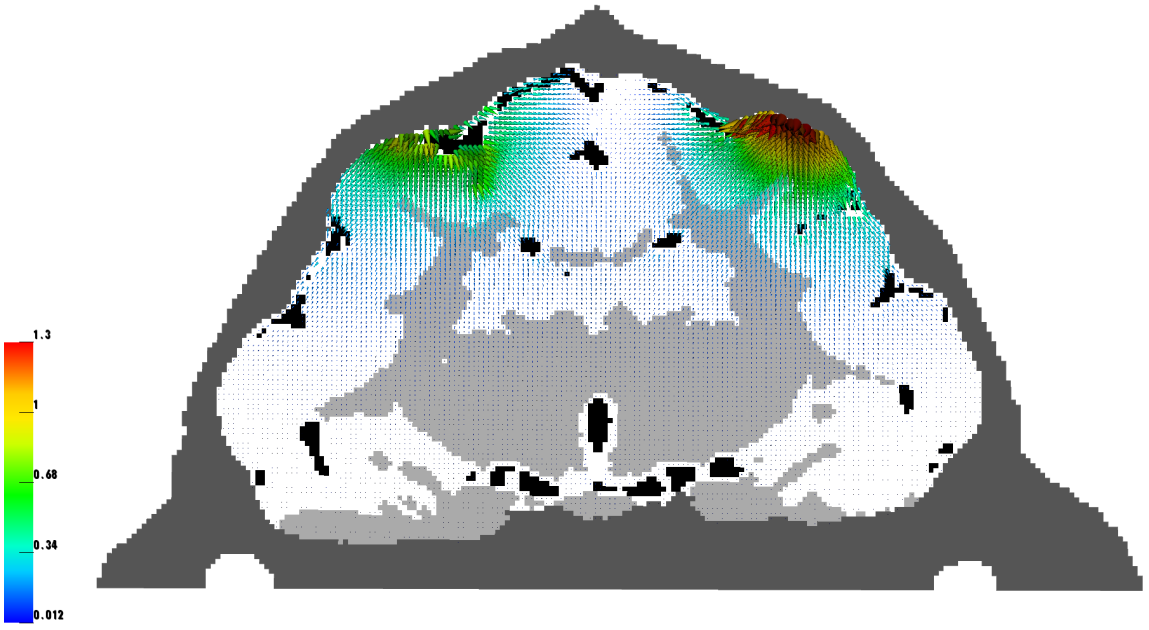

Figure 7.6: Front-back stimulation

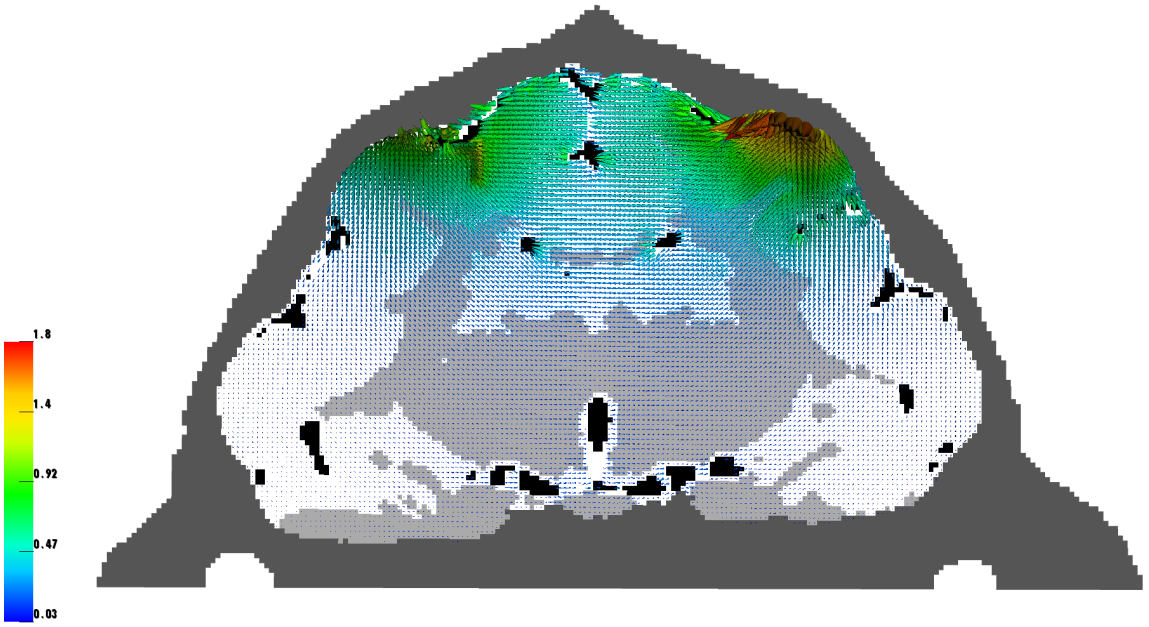

Figure 7.7: Right-left stimulation

As seen in the figures 7.6, and 7.7 we can visually validate the stimulation. Both electric fields are aligned from the cathodal to the anodal electrodes.

7.3 Advanced electrode setup

We will elaborate a more complex electrode configuration which allows us to use an optimized stimulation protocol to stimulate a desired region in the brain.

7.3.1 Electrode setup

We use 35 electrodes distributed over the head to cover most of the skull. We reduced the amount of electrodes compared to the human head model due to practical reasons as a ferret head is way smaller than a human head.

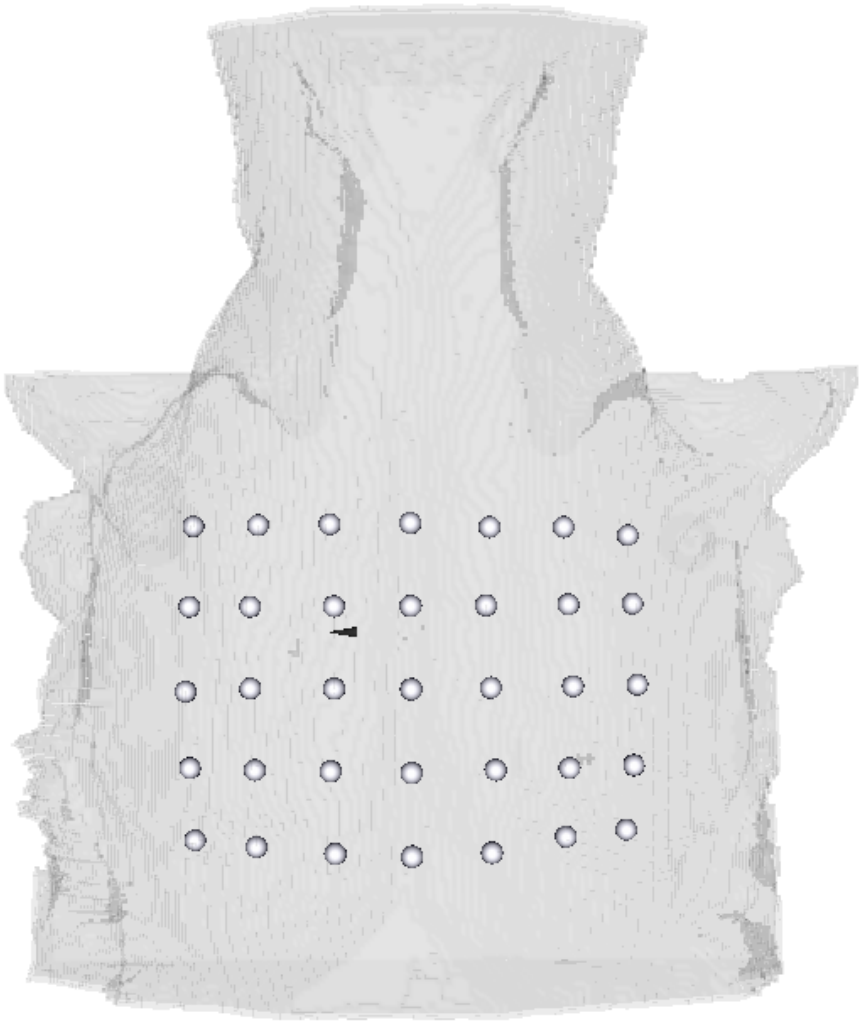

Figure 7.8: Advanced electrode setup

7.3.2 Simulation

As target we use surface near tangential target.

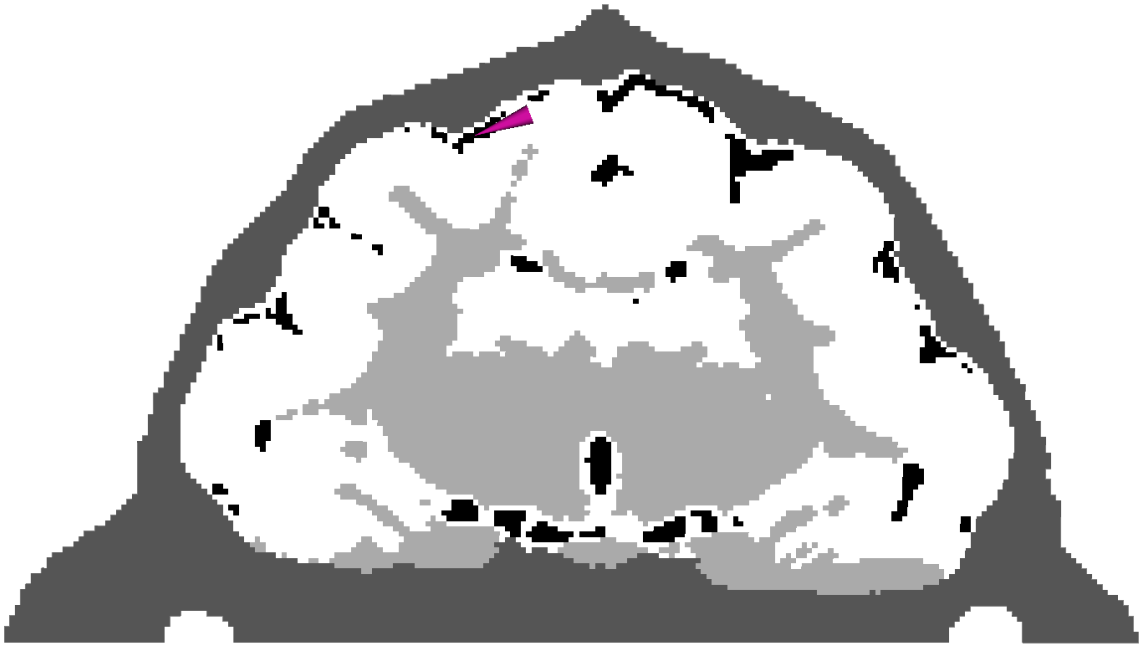

Figure 7.9: Target

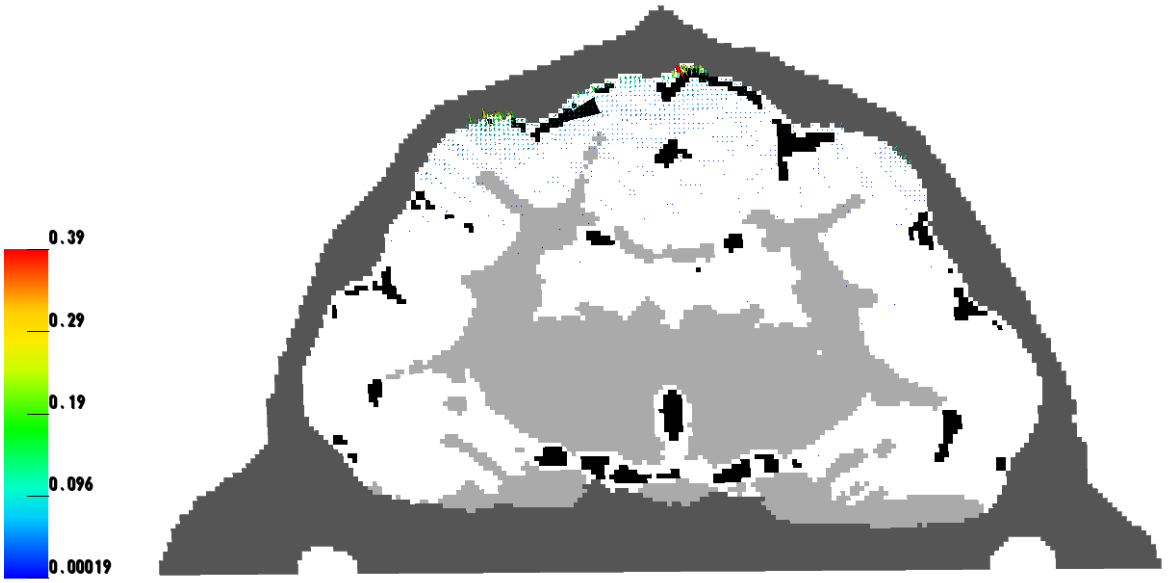

Figure 7.10: Optimization with LCMV

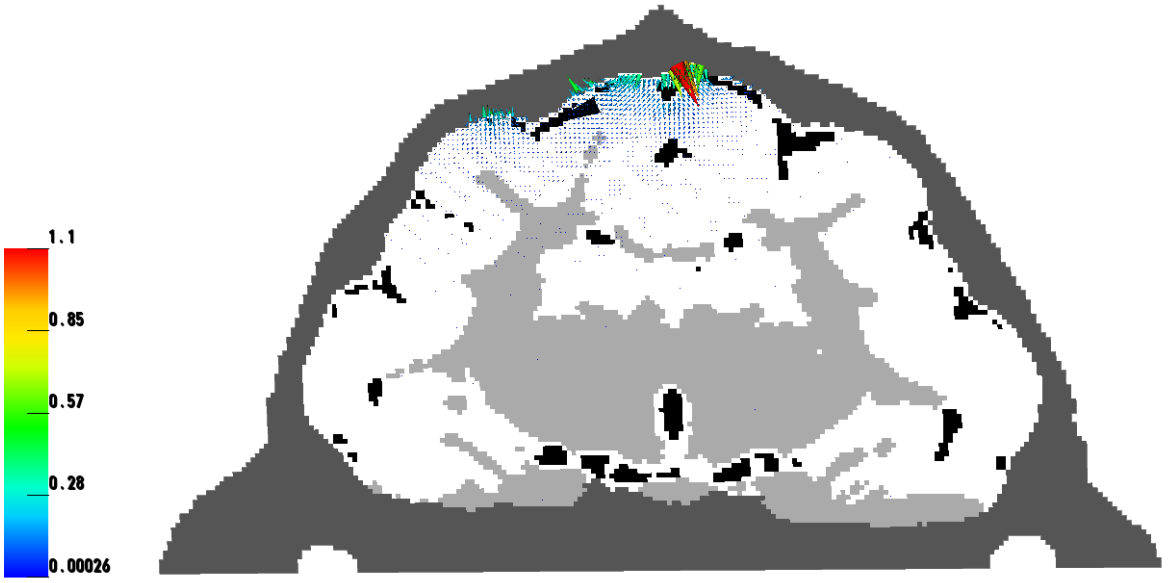

Figure 7.11: Optimization with LS

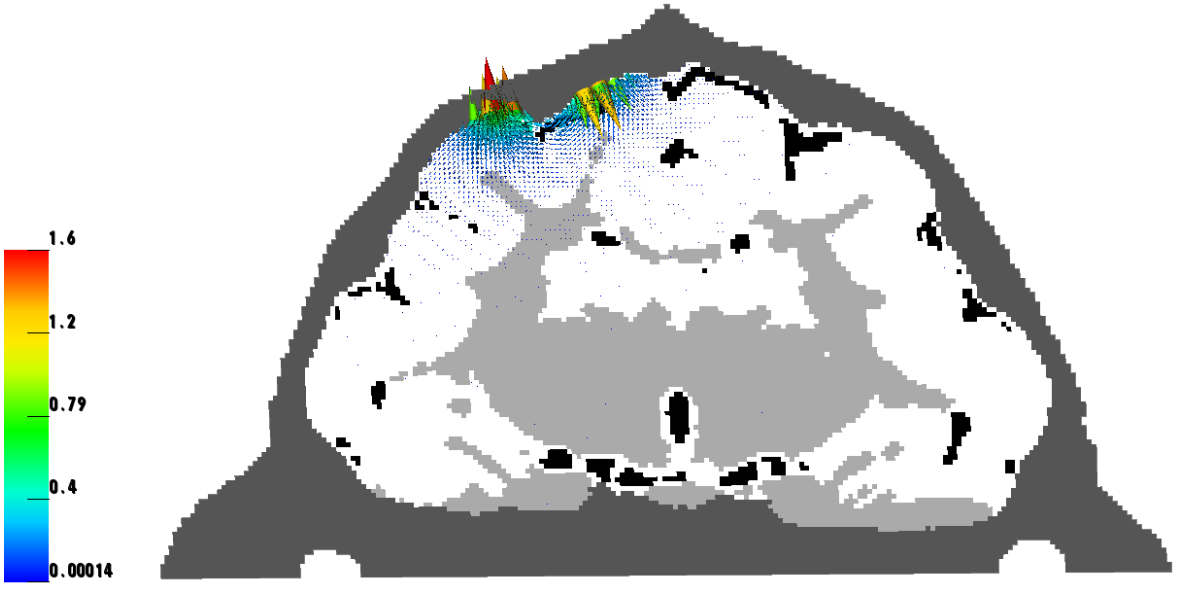

Figure 7.12: Optimization with max. Intensity

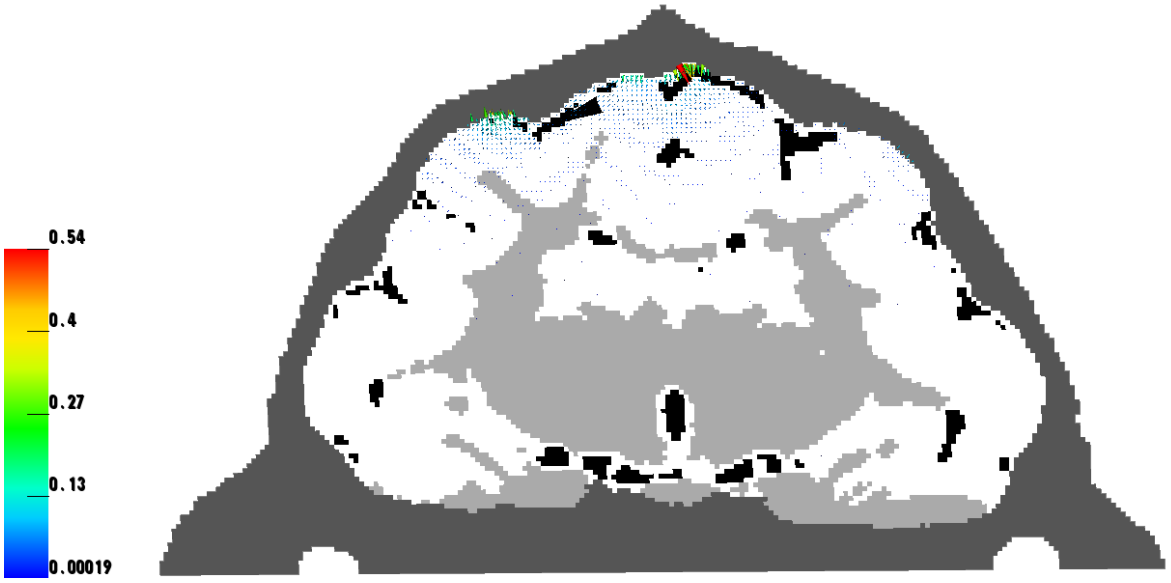

Figure 7.13: Optimization with ADMM

7.3.3 Evaluation

		$[Am^{-2}]$				[%]
Method	IT	INT	DIR	FOC	cEMD	PAR
LCMV	0.06202	0.00330	0.6202	18.79	2140	**100%**
ADMM-L1R	0.05995	0.00319	0.05834	18.79	1245	97.31%
W-LS	0.12218	0.00397	0.09192	30.77	1169	75.23%
max. Intensity	**0.24434**	0.00453	0.24416	**53.93**	**564**	99.92%

In this simulation we see that the max. Intensity approach yields best results with regards to the characteristic values. It has the highest IT and FOC while the PAR is nearly perfect.
These results quite differ from the simulation on a human head model which could be caused by the stimulation without a scalp. A scalp has a much higher conductivity than a skull. This causes the current directly flowing into the head despite being blurred by the skin.

8 Summary

In this thesis we provided an insight in simulation of tDCS and optimization of its stimulation protocol.

EEG and tDCS

With the Helmholtz reciprocity principle we made a bridge between EEG-source reconstruction and brain stimulation via tDCS. We showed the usage of the lead field, which is highly used in EEG source reconstruction, in optimization of the tDCS stimulation protocol.

Mathematical problem

We defined the mathematical problem of tDCS. We discussed a source and sink free volume conductor and described the relation between current density and the electric field. This would provide us a partial differential equation on which we can base a volume conduction model that help use to simulate tDCS.

Optimization

With regards to stimulation we introduced approaches like alternating direction and methods of multiplier, least square, minimum variance linearly constrained and the maximal intensity, to optimize the stimulation protocol.

Simulation and evaluation

We introduced a human and a ferret head model. These are based and MRI-measurements which allowed a sufficient segmentation of different head tissues. Based on these models

we could perform different simulations. To compare the performed simulation we introduced different unitless characteristic numbers on which we could compare the different approaches.

First of all we compared the different performances of the approaches on different single targets in the human head. In addition we simulated a two-target setup and evaluated the different outcomes of each approach. As last simulation on the human head model we simulated a misspecification of the target's angle to get and insight to the robustness of the different approaches.

A simple stimulation simulation was performed on the ferret head model. We showed that it was possible to achieve reasonable results on another species than a human. Furthermore we did a stimulation optimization on an advanced electrode setup with the head model of the ferret to get a further insight of the optimization approaches.

As a conclusion we can't provide evidence for an overall best approach for tDCS protocol optimization. As discussed in this thesis the needs of the experiment have to be specified and actually how an optimal solution would look like. So as an optimal solution is defined, the evaluation of these simulations can provide the optimal approach.

9 Outlook

In this thesis we focused on the optimization of the stimulation protocol of tDCS, however there are more parameters that can be optimized.

First of all the electrode configuration is a crucial part of the stimulation. One can imagine a very sparse setup i.e. four electrodes won't provide as good results as a 74 electrode configuration. However the location of the electrodes isn't arbitrary. In an extreme case no electrode is located on the head surface near our target and therefore the stimulation protocol wouldn't optimal with regards to location of the electrode, focality and stimulation direction of the target.

Another topic that can be investigated is different approaches of tMS or even combined tMS/tDCS, as a multi-coil set up of tMS which is also a well known and used technique [31] [32]. In [2] we can find optimization approaches for tMS and combined tMS/tDCS. The interest of more optimization approaches with regards to these techniques and the simulation and evaluation of them could also be a research topic.

List of Figures

Bibliography

[1] J. P. Dmochowski, A. Datta, M. Bikson, Y. Su, and L. C. Parra, "Optimized multi-electrode stimulation increases focality and intensity at target," *Journal of neural engineering*, vol. 8, no. 4, p. 046011, 2011. 1, 15, 34

[2] S. Wagner, "Phd-thesis: Optimizing tcs and tms multi-sensor setups using realistic head models," 2015. 1, 8, 10, 11, 16, 36, 69

[3] "Neuron," *http://www.enchantedlearning.com/subjects/anatomy/brain/Neuron.shtml*, July 2015. 4

[4] C. M. A. Carie Ann Braun, *Pathophysiology: Functional Alterations in Human Health*. Lippincott Williams Wilkins, 2007. 3

[5] "Action potential," *https://upload.wikimedia.org/wikipedia/commons/thumb/4/4a/Action_potential.svg/300px-Action_potential.svg.png*, July 2015. 4

[6] A. Parent, "Giovanni aldini: from animal electricity to human brain stimulation," *The Canadian Journal of Neurological Sciences*, vol. 31, no. 04, pp. 576–584, 2004. 4

[7] M. A. Nitsche, A. Schauenburg, N. Lang, D. Liebetanz, C. Exner, W. Paulus, and F. Tergau, "Facilitation of implicit motor learning by weak transcranial direct current stimulation of the primary motor cortex in the human," *Journal of cognitive neuroscience*, vol. 15, no. 4, pp. 619–626, 2003. 4, 5

[8] M. Nitsche and W. Paulus, "Excitability changes induced in the human motor cortex by weak transcranial direct current stimulation," *The Journal of physiology*, vol. 527, no. 3, pp. 633–639, 2000.

[9] L. Marshall, M. Mölle, M. Hallschmid, and J. Born, "Transcranial direct current stimulation during sleep improves declarative memory," *The Journal of neuroscience*, vol. 24, no. 44, pp. 9985–9992, 2004. 4

[10] M. Akhtari, H. Bryant, A. Mamelak, E. Flynn, L. Heller, J. Shih, M. Mandelkem, A. Matlachov, D. Ranken, E. Best, *et al.*, "Conductivities of three-layer live human skull," *Brain topography*, vol. 14, no. 3, pp. 151–167, 2002. 4, 32

[11] K. E. Hoy, S. L. Arnold, M. R. Emonson, Z. J. Daskalakis, and P. B. Fitzgerald, "An investigation into the effects of tdcs dose on cognitive performance over time in patients with schizophrenia," *Schizophrenia research*, vol. 155, no. 1, pp. 96–100, 2014. 4

[12] R. Ferrucci, F. Mameli, I. Guidi, S. Mrakic-Sposta, M. Vergari, S. Marceglia, F. Cogiamanian, S. Barbieri, E. Scarpini, and A. Priori, "Transcranial direct current stimulation improves recognition memory in alzheimer disease," *Neurology*, vol. 71, no. 7, pp. 493–498, 2008. 4

[13] P. S. Boggio, S. Zaghi, M. Lopes, and F. Fregni, "Modulatory effects of anodal transcranial direct current stimulation on perception and pain thresholds in healthy volunteers," *European Journal of Neurology*, vol. 15, no. 10, pp. 1124–1130, 2008. 4

[14] R. Sparing, M. Thimm, M. Hesse, J. Küst, H. Karbe, and G. Fink, "Bidirectional alterations of interhemispheric parietal balance by non-invasive cortical stimulation," *Brain*, vol. 132, no. 11, pp. 3011–3020, 2009. 4

[15] O. D. Creutzfeldt, G. H. Fromm, and H. Kapp, "Influence of transcortical dc currents on cortical neuronal activity," *Experimental neurology*, vol. 5, no. 6, pp. 436–452, 1962. 6, 53

[16] N. Jost, L. Virág, M. Bitay, J. Takács, C. Lengyel, P. Biliczki, Z. Nagy, G. Bogáts, D. A. Lathrop, J. G. Papp, *et al.*, "Restricting excessive cardiac action potential and qt prolongation a vital role for iks in human ventricular muscle," *Circulation*, vol. 112, no. 10, pp. 1392–1399, 2005. 6

[17] C. Wolters, "Mathematical methods in bioelectromagnetism and in the analysis of biosignals," 2014. 7

[18] S. Boyd and L. Vandenberghe, *Convex optimization*. Cambridge university press, 2004. 11

[19] V. C. Klema and A. J. Laub, "The singular value decomposition: Its computation and some applications," *Automatic Control, IEEE Transactions on*, vol. 25, no. 2, pp. 164–176, 1980. 12

[20] Y. Rubner, C. Tomasi, and L. J. Guibas, "The earth mover's distance as a metric for image retrieval," *International journal of computer vision*, vol. 40, no. 2, pp. 99–121, 2000. 12

[21] S. Boyd, N. Parikh, E. Chu, B. Peleato, and J. Eckstein, "Distributed optimization and statistical learning via the alternating direction method of multipliers," *Foundations and Trends® in Machine Learning*, vol. 3, no. 1, pp. 1–122, 2011. 19

[22] Ümit Aydin, "Phd-thesis: Combined eeg and meg source analysis of epileptiform activity using calibrated realistic finite element head models," 2015. 31

[23] M. Dannhauer, B. Lanfer, C. H. Wolters, and T. R. Knösche, "Modeling of the human skull in eeg source analysis," *Human brain mapping*, vol. 32, no. 9, pp. 1383–1399, 2011. 32

[24] S. B. Baumann, D. R. Wozny, S. K. Kelly, and F. M. Meno, "The electrical conductivity of human cerebrospinal fluid at body temperature," *Biomedical Engineering, IEEE Transactions on*, vol. 44, no. 3, pp. 220–223, 1997. 32

[25] C. Ramon, P. Schimpf, J. Haueisen, M. Holmes, and A. Ishimaru, "Role of soft bone, csf and gray matter in eeg simulations," *Brain topography*, vol. 16, no. 4, pp. 245–248, 2004. 32

[26] R. Tibshirani, "Regression shrinkage and selection via the lasso," *Journal of the Royal Statistical Society. Series B (Methodological)*, pp. 267–288, 1996. 35

[27] M. Grant, S. Boyd, and Y. Ye, *Disciplined convex programming*. Springer, 2006. 36

[28] L. J. Bindman, O. Lippold, and J. Redfearn, "Long-lasting changes in the level of the electrical activity of the cerebral cortex produced by polarizing currents," 1962. 6, 53

[29] J. Fox and R. Marini, *Biology and Diseases of the Ferret*. Wiley, 2014. 58

[30] D. Gullmar, J. Haueisen, M. Eiselt, F. Gießler, L. Flemming, A. Anwander, T. Knosche, C. H. Wolters, M. Dumpelmann, D. S. Tuch, *et al.*, "Influence of anisotropic conductivity on eeg source reconstruction: investigations in a rabbit model," *Biomedical Engineering, IEEE Transactions on*, vol. 53, no. 9, pp. 1841–1850, 2006. 59

[31] A. Tzabazis, C. M. Aparici, M. C. Rowbotham, M. B. Schneider, A. Etkin, and D. C. Yeomans, "Shaped magnetic field pulses by multi-coil repetitive transcranial

magnetic stimulation (rtms) differentially modulate anterior cingulate cortex responses and pain in volunteers and fibromyalgia patients," *Mol Pain*, vol. 9, no. 1, p. 33, 2013. 69

[32] L. Hernandez-Garcia, A. Grbic, E. Michielssen, and L. Gomez, "Multi-coil transcranial magnetic stimulation," 2012. US Patent App. 14/130,707. 69

Plagiatserklärung der / des Studierenden

Hiermit versichere ich, dass die vorliegende Arbeit über _____ _____ selbstständig verfasst worden ist, dass keine anderen Quellen und Hilfsmittel als die angegebenen benutzt worden sind und dass die Stellen der Arbeit, die anderen Werken – auch elektronischen Medien – dem Wortlaut oder Sinn nach entnommen wurden, auf jeden Fall unter Angabe der Quelle als Entlehnung kenntlich gemacht worden sind.

_____
(Datum, Unterschrift)

Ich erkläre mich mit einem Abgleich der Arbeit mit anderen Texten zwecks Auffindung von Übereinstimmungen sowie mit einer zu diesem Zweck vorzunehmenden Speicherung der Arbeit in einer Datenbank einverstanden.

_____
(Datum, Unterschrift)